

1 **Observed salinity fields in the surface layer of the Arctic Ocean and statistical**
2 **approaches to predicting large-scale anomalies and patterns**

3 Ekaterina A. Cherniavskaia¹, Ivan Sudakov^{2,*}, Kenneth M. Golden³, Courtenay Strong⁴ and
4 Leonid A. Timokhov¹

5 ¹Department of Oceanography, Arctic and Antarctic Research Institute, Bering str. 38, St.
6 Petersburg, 199397 Russia.

7 ²Department of Physics, 300 College Park, SC 101B, University of Dayton, Dayton, OH
8 45469-2314 USA

9 ³Department of Mathematics, University of Utah, 155 S 1400 E, Room 233, Salt Lake City,
10 UT 84112-0090 USA.

11 ⁴Department of Atmospheric Sciences, University of Utah, 135 S 1460 E, Room 819, Salt Lake
12 City, UT 84112-0090 USA.

13 * corresponding author:

14 email: isudakov1@udayton.edu

15

16 **Abstract**

17 Significant salinity anomalies have been observed in the Arctic Ocean surface layer during the
18 last decade. Our study is based on an extensive gridded data set of winter salinity in the upper
19 50-meter layer of the Arctic Ocean for the periods 1950-1993 and 2007-2012, obtained from
20 approximately 20,000 profiles. We investigate the inter-annual variability of the salinity fields,
21 identify predominant patterns of anomalous behavior and leading modes of variability, and
22 develop a statistical model for the prediction of surface layer salinity. The statistical model is
23 based on linear regression equations linking the principal components of surface layer salinity
24 obtained through Empirical Orthogonal Function (EOF) decomposition with environmental
25 factors, such as atmospheric circulation, river runoff, ice processes, and water exchange with

26 neighboring oceans. Using this model, we obtain prognostic fields of the surface layer salinity
27 for the winter period 2013-2014. The prognostic fields generated by the model show tendencies
28 of surface layer salinification which were also observed in previous years. Although data that
29 were used are proprietary and have gaps, they provide the most spatiotemporally detailed
30 observational resource for studying multidecadal variations in basin-wide Arctic salinity. Thus
31 there is community value in the identification, dissemination, and modeling of the principal
32 modes of variability in this salinity record.

33

34 **Keywords:** Arctic Basin, surface layer, patterns, salinity anomalies, empirical orthogonal
35 functions, gridding.

36

37 1. Introduction

38 The Arctic Ocean is very sensitive to changing environmental conditions. Its surface
39 layer is a key component of the Arctic climate system, which serves as the dynamic and
40 thermodynamic link between the atmosphere and the underlying waters (Carmack, 2000).
41 Thermohaline characteristics of the surface layer are markedly influenced by atmospheric and
42 sea ice processes, and wind and buoyancy forcing on this important layer ultimately impact the
43 entire upper ocean (Cronin and Sprintall, 2001). The rejection of salt during sea ice formation
44 strongly impacts upper ocean salinity, so that the stability and development of the ice cover are
45 closely associated with the thermohaline properties of the upper ocean, such as the depth of the
46 mixed layer and halocline. In this context, the Arctic Ocean surface layer is a critical indicator
47 of climate change (Toole et al., 2010).

48 Here, salinity is chosen as the main characteristic of thermohaline structure variations
49 of the Arctic Ocean surface layer because, at high latitudes, it mainly determines the density
50 structure (Weyl, 1968; Morison & Smith, 1981; Walin, 1985). The thermohaline structure of

51 the Arctic Ocean surface layer has undergone significant changes in recent years (Macdonald
52 et al., 2005). Of particular interest is the great salinification of the surface layer of the Eurasian
53 and Makarov Basins in the early 1990s – a phenomenon unprecedented in the record back to
54 1950 (Figure 1). One hypothesis for this is that the increase of Arctic atmospheric cyclone
55 activity in the 1990s led to a large change in the salinity in the Eurasian Basin through changes
56 in river inflow, and increased brine formation due to changes in Arctic sea ice formation
57 (Dickson, 1999; Polyakov et al., 2008). The other reason for salinification is the influence of
58 Atlantic waters (AW), which by 2007 became warmer by about 0.24°C than they were in the
59 1990s. Observations show that increases in Arctic Ocean salinity have accompanied this
60 warming as it was associated with significant shoaling of the upper AW boundary and
61 weakening of the upper-ocean stratification in the Eurasian Basin as well. That led to facilitated
62 exchange between AW and the upper layer (Polyakov et al., 2010). However, recent
63 observations also show that the upper ocean of the Eurasian Basin was appreciably fresher in
64 2010 than it was in 2007 and 2008 (Timmermans et al., 2011).

65 In addition, there have been observations of surface layer freshening in the Canada
66 Basin. Jackson et al. (2012) emphasized that processes related to warming and freshening the
67 surface layer in this region had transformed the water mass structure of the upper 100 m. With
68 these changes, energy absorbed during summer can enter the deepening winter mixed layer and
69 melt sea ice.

70 The problem of variability of Arctic Ocean salinity is challenging from a theoretical
71 perspective. For example, Lique et al. (2009) performed an analysis of the variability of Arctic
72 freshwater content informed by a global ocean/sea-ice model. The authors uncovered important
73 spatial contrasts in the influence of velocity and salinity fluctuations on ocean freshwater
74 transport variability. They conclude that variations of salinity (controlling part of the Fram
75 freshwater export) arise from the sea ice formation and melting north of Greenland. Jahn et al.

76 (2012) compared simulations from ten global ocean-sea ice models of Arctic freshwater, and
77 concluded that improved simulations of salinity variability are required to advance
78 understanding of liquid freshwater export.

79 Improving the representation of the salinity distribution is crucial. However inclusion,
80 representation, and parametrization of a number of processes is required (Steele et al., 2001;
81 Komuro, 2014). For example, in many global ocean-sea ice models, salt is rejected in the first
82 level of the ocean model during ice formation, while in reality, the salt is distributed in the
83 mixed layer and below (Nguyen et al., 2009).

84 The transfer of fresh water and sea ice from the Arctic Ocean to the North Atlantic are
85 significant components of global ocean circulation (Haak et al., 2003; Gelderloos et al., 2012).
86 Thus, the investigation of the variability of the surface layer can make a significant contribution
87 to understanding ocean-climate feedback. In particular, abrupt changes in surface-layer salinity
88 may lead to critical transitions in patterns of global ocean circulation, such as convection shut
89 downs and climate disruptions (Hall & Stouffer, 2001; Gelderloos et al., 2012). A robust
90 conceptual statistical model may help to describe features of anomalies in salinification of the
91 Arctic Ocean, which are key players in the formation of surface-layer salinity patterns. In this
92 case, investigation of the structure of patterns and quality of anomalies leads to a better
93 understanding of possible critical transitions in patterns of global ocean circulation. Variations
94 of Arctic Ocean surface-layer salinity have complex spatial and temporal structures, which are
95 affected by many external factors. Our aim is to distinguish the most significant factors that led
96 to recent changes in surface-layer salinity patterns.

97 Here, we present a statistical model for Arctic Ocean salinity fields based on multiple
98 linear regression analysis, which builds on ideas presented in prior studies (e.g., Timokhov et
99 al., 2012). This statistical model of variability of Arctic Ocean winter salinity in the 5–50 meter
100 layer is used as a method of reconstruction of observed winter salinity fields presented in

101 Pokrovsky and Timokhov (2002). The model is based on an Empirical Orthogonal Function
102 (EOF) decomposition of the salinity data (e.g., Hannachi et al., 2007), and a multiple
103 correlation analysis of the time series associated with the first three leading modes, or principal
104 components (PC); see Appendix Figure A2 for a schematic diagram of the model. The
105 contribution of atmospheric factors and hydrological processes in the spatial distribution of
106 surface-layer salinity was interpreted by determining the structure of the multiple correlation
107 equations. The variability patterns and relationships identified through the statistical analysis
108 and modeling inform a conceptual model for principal drivers of Arctic salinity.

109

110 **2. Methods**

111 **2.1. Data Set**

112 This study is based on a collection of more than 9,800 instantaneous temperature and
113 salinity profiles, with data available at the standard levels (5, 10, 25, 50, 75, 100, 150, 200, 250,
114 300, 400, 500, 750, 1000 and so on every 500 meters), collected between 1950-1993. The data
115 were obtained from the Russian Arctic and Antarctic Research Institute (AARI) database,
116 which was also used in the creation of the joint U.S. Russian Atlas of the Arctic Ocean for
117 winter (Timokhov and Tanis, 1997). This is complemented by data made available over the
118 period 2007-2012 from the expeditions of the International Polar Year (IPY) and afterward,
119 which consist of Conductivity Temperature Depth (CTD) and eXpendable Conductivity
120 Temperature Depth (XCTD) data, as well as data from the Ice-Tethered Profiler (ITP)-buoys
121 (more than 14,600 stations in total). The average vertical resolution of all these profiles was 1
122 m. The AARI database was first introduced by Lebedev et al. (2008). In areas where
123 observations were missing, temperature and salinity data were reconstructed in a regular grid
124 for the period 1950 to 1989 as detailed in the next subsection. Thus, the working database is
125 represented by grids with 200-km horizontal spacing, covering the deep part of the Arctic

126 Ocean (with depths of more than 50 m). According to Treshnikov (1959), Rudels et al. (1996,
127 2004), and Korhonen et al. (2013), the average thickness of the Arctic Ocean mixed layer for
128 the winter season is about 50 m. A description of the data sources for other physical parameters,
129 used as predictors for the statistical model, can be found in Table 1.

130 The database used in this study belongs to the Oceanography Department of the Arctic
131 and Antarctic Research Institute and it is not freely available. To mitigate the related issues we
132 provide additional data description. Table A1 in the Supplementary Material contains a list of
133 the expeditions and number of stations that were used for reconstruction and gridding of
134 salinity fields. Figure A1 shows the overall observation density and the year associated with
135 each observation. The data exhibit a spatiotemporal non-uniformity that is undesirable but
136 expected given the logistical challenges associated with recovering long-term observations of
137 Arctic salinity. While this data set has gaps and is proprietary, it provides the most
138 spatiotemporally detailed observational resource for studying multidecadal variations in basin-
139 wide Arctic salinity. This manuscript is motivated by the potential to advance understanding
140 through identification, dissemination, and modeling of the principal modes of variability in
141 these long-term salinity observations.

142 Gridded fields of surface winter salinity were compared with fields from the Pan-Arctic
143 Ice-Ocean Modeling and Assimilation System (PIOMAS; Zhang and Rothrock, 2003, Lindsay
144 and Zhang, 2006) for their overlapping period 1978-1993 (dashed curves, Figure 1). PIOMAS
145 is a coupled ice-ocean model which uses data assimilation methods for ice concentration and
146 ice velocity. Forced by atmospheric observations, its output is available for 1978 to near present
147 and is widely used as a reference for Arctic variables with limited long-term observations
148 including salinity and sea ice thickness. Maps of long-term means for both data sets are similar
149 (Figure 2a and Figure A3a), with a correlation coefficient of 0.88. Nevertheless, PIOMAS data
150 generally provide higher salinity values for the Amerasian Basin (Canada Basin together with

151 Makarov Basin) for the overlapping period (Figure 1). The associated variance maps are also
 152 significantly correlated with each other (correlation coefficient $R=0.36$; statistical significance
 153 level $p=0.05$) but exhibited some salient differences (Figure A4). In particular, a high variance
 154 zone along the Lomonosov Ridge is prominent in the AARI data set, but is absent in PIOMAS
 155 data. PIOMAS instead features several centers of high variance along the shelf.

156 To test for artifacts from the data gaps and the interpolation procedure (reviewed in the
 157 next subsection), we make several comparisons across methods and to independent data sets in
 158 the subsections to follow. For example, we also performed the EOF analysis with and without
 159 the additional 2007-2012 period, and report only modest change to the resulting modes of
 160 variability (Section 3.1). In Section 3.1, we also compare EOFs from the AARI data to those
 161 from PIOMAS.

162 2.2. Field reconstruction and interpolation

163 To provide temporal and spatial continuity, we have unified existing data sets using
 164 reconstruction and gridding. The technique of computing gridded fields for the period from
 165 1950-1993 was described by Lebedev et al. (2008), and is summarized here.

166 These techniques are based on the method of ocean field reconstruction, proposed by
 167 Pokrovsky and Timokhov (2002). This method, which was used to obtain gridded salinity
 168 fields, is given by

$$169 \quad \begin{aligned} z_i &= z_i^{(r)} + e_i, \quad \langle z_i z_j \rangle = \sigma_{x_i x_j}, \quad \langle z_i e_i \rangle = 0, \\ \langle e_i \rangle &= 0, \quad \langle e_i e_j \rangle = \delta_{ij} \sigma_e^2 = \sigma_{e_{ij}}^2. \end{aligned} \quad (1)$$

170 Here $z(t, x)$ is the measured value of an oceanographic variable (e.g., temperature or salinity),
 171 and is a random function of time t and spatial coordinates x ; i and j are the nodes of the irregular
 172 data grid; the notation $\langle \dots \rangle$ denotes the ensemble average of a value. We can write the observed
 173 value of $z(t, x)$ as the sum of a true value $z^{(r)}(t, x)$ of the oceanographic variable and an
 174 observational error $e(t, x)$. In addition, we introduce $\sigma_{x_i x_j}$ as a standard deviation of spatial

175 coordinates and $\sigma_{e_{ij}}^2$ as a standard deviation of errors. We also propose that $z_i^{(r)}$ has spatial
 176 correlations to the oceanographic parameters; that a systematic error is not identified; a
 177 standard deviation of error (σ_e^2) does exist; and $\delta_{ij} = \begin{cases} 0, & \text{if } i \neq j \\ 1, & \text{if } i = j \end{cases}$ is the Kronecker delta.

178 Biorthogonal decomposition of the oceanographic variable can help to identify the
 179 connections between spatial and temporal distributions within the data:

$$180 \quad z(t_j, x_i) = \sum_k c_k^j f_k(x_i) + e(t_j, x_i), \quad (2)$$

181 where $f_k(x_i)$ is the spatial EOF, and c_k^j is the calculated coefficient or so-called k^{th} principal
 182 component (PC).

183 As the next step we approximate the EOF through linear combinations (with
 184 coefficients b_{kl}) of convenient analytical functions $P_l(x_i)$ (for example, polynomials, splines,
 185 etc.):

$$186 \quad f_k(x_i) = \sum_l b_{kl} P_l(x_i) \quad . \quad (3)$$

187 Thus, the modified biorthogonal decomposition can be written as

$$188 \quad z(t_j, x_i) = \sum_k d_l^j P_l(x_i) + e(t_j, x_i), \quad (4)$$

$$189 \quad \text{where } d_l^j = \sum_k b_{kl} c_k^j \quad .$$

190 The main goal of this spectral analysis method is to estimate the coefficients of spectral
 191 decomposition $\{c_k^j\}$ and $\{b_{kl}\}$, in order to identify dominant modes of behavior. In this case,
 192 we rewrite formula (2) in the following matrix form:

$$193 \quad Z = F \bullet C + e, \quad (5)$$

194 where \bullet denotes matrix multiplication.

195 The matrix F is formed by the values of the EOF, the matrix Z is composed of the
 196 totality of the measurement data at the points of the observation net x_i , and the matrix e is filled
 197 out by observational error values.

198 The system of linear equations (5) with respect to the unknown coefficients c_k^j can be
 199 solved on the basis of the *a priori* statistical information (1) with the use of the standard
 200 estimation of the least squares method. A formula for the estimation of the matrix of the
 201 unknown coefficients C was obtained in (Pokrovsky and Timokhov, 2002), and is written

$$202 \hat{C} = (F^T \cdot K_e^{-1} \cdot F + K_c^{-1})^{-1} F^T \cdot K_e^{-1} \cdot Z', \quad (6)$$

203 where X^{-1} and X^T denote the inverse and transpose of a matrix X , respectively. The covariance
 204 matrix of errors of the expansion coefficients K_c is a diagonal matrix composed of eigenvalues
 205 of the covariance matrix K_z . Here, the matrixes K_z and K_e are covariance matrices of the
 206 standard deviation of spatial coordinates and the standard deviation of errors, respectively.

207 In order to obtain an estimate of the unknown variables at the nodes of the regular grid
 208 \tilde{x}_i , it is necessary to interpolate the EOF into the corresponding nodes of the grid and obtain a
 209 new matrix \tilde{F} of the EOF, a new matrix \tilde{C} of decomposition coefficients, and new matrix \tilde{e} of
 210 observational errors. Using the matrix \tilde{F} obtained in this way and the estimates of the
 211 coefficients \hat{C} from formula (6), from the matrix relationship

$$212 \tilde{Z} = \tilde{F} \cdot \tilde{C} + \tilde{e}, \quad (7)$$

213 we obtain an estimate of the unknown parameters at the nodes of a regular grid. Simultaneously
 214 with the salinity fields in the nodes of a regular grid, we can also calculate the covariance
 215 matrices of the errors of estimations obtained from the following equations:

$$216 K_{\hat{c}} = \left(I + \left(K_c \cdot (\tilde{F}^T \cdot \tilde{K}_e^{-1} \cdot \tilde{F}) \right) \right)^{-1} \cdot K_c$$

$$217 K_{\hat{z}} = \tilde{F} \cdot K_z \cdot \tilde{F}^T, \quad (8)$$

218 where I is the identity matrix and \tilde{K}_e^{-1} is the covariance matrix of the observation error
 219 expanded over the regular grid x_i .

220 This approach is a combination of singular value decomposition and statistical
 221 regularization. These coefficients (modes) can be linked to the real physical processes that
 222 influence salinity as presented in Section 2.3. Preparation of the average salinity field data for

223 2007-2012 consisted of several stages as detailed in the Appendix. First, we checked the data
224 for random errors. Then, we used linear interpolation and assimilated the real plane with the
225 field data through the virtual plane of data. Next, we constructed an interpolation via a grid of
226 nodes (separately for each plane). The gaps in the data for uncovered sites were filled with
227 climatic values from the Joint U.S.-Russian Atlas of the Arctic Ocean (Timokhov and Tanis,
228 1997).

229 **2.3. Statistical approach**

230 Here we describe the approaches to data analysis which were used for physical
231 interpretation of our statistical model. Polyakov et al. (2010), Rabe et al. (2011), and Morison
232 et al. (2012) have emphasized that the thermohaline structure of the surface layer has undergone
233 significant change over the last decade. However, it is not clear what physical processes led to
234 these changes or what the future trends may be.

235 The analysis of the variability of the surface layer (including salinity fields) of the
236 Arctic Ocean may be based on a decomposition using EOFs. This approach is useful in our
237 case because decomposition by EOF analysis gives modes (spatial patterns) and principal
238 component (PC) time series, which allow us to divide the variability into spatial and temporal
239 components. Each mode describes a certain fraction of the total variance of the initial data, and
240 the EOFs are conventionally ordered so that the first EOF explains the most variance and
241 subsequent EOFs explain progressively less variance (Hannachi et al., 2007). The first 3 modes
242 describe more than half the variance of the analyzed fields as further detailed below, which
243 allows significant compressing of the information contained in the original data (Hannachi et
244 al., 2007; Borzelli and Ligi, 1998). The EOF decomposition was carried out for the average
245 salinity fields for the layer 5-50 m, yielding PCs for the periods of 1950-1993 and 2007-2012.

246 Multiple linear regression was used to model the PC time series to identify predictors
247 that determined variability of the salinity fields. The regression equations can give projections

248 of future changes because the predictors lead the salinity field by various temporal lags. The
249 statistical model is characterized by a system of linear regression equations constructed for the
250 first three PCs. The candidate predictors were as follows: atmospheric circulation indices (AO
251 and AD; see Table 1) calculated for winter (October-March to cover the period of active ice
252 formation) and summer (July-September to cover the period of active ice melting), river runoff,
253 the area of the ice-free surface in Arctic seas in September, and water exchange with the Pacific
254 and Atlantic Oceans. For the latter two water exchanges, we used the PDO and AMO indices
255 as respective proxies because of their influence on the temperature and salinity of water, which
256 is entering through the Bering Strait and the Faeroe-Shetland Strait to the Arctic Ocean (Zhang
257 et al., 2010; Dima and Lohmann, 2007). Atmospheric indices were averaged by different time
258 periods within indicated winter and summer seasons. The optimal periods of averaging for a
259 particular index were chosen on the basis of maximal correlations with PCs.

260

261 **3. Results**

262 **3.1. Decomposition of surface layer salinity fields by EOF**

263 As a result of EOF decomposition of the salinity fields for the 5-50 m layer, we obtained
264 two sets of modes and PCs – one for the period of 1950-1993 (series 1), and one for the same
265 period adding the years 2007-2012 (series 2). North's rule of thumb states the following: if the
266 sampling error in an eigenvalue is comparable to the distance to a neighboring eigenvalue, then
267 the sampling error of the EOF will be comparable to the size of the neighboring EOF (North et
268 al., 1982). Based on this rule, the first three modes were accepted for further analysis as
269 physically significant. The first three modes obtained by the decomposition of series 1 describe
270 more than 55% of the total dispersion of the initial fields. The first three modes of series 2
271 describe more than 61% of the total dispersion. Nevertheless, the first modes for both
272 decompositions have very similar shapes. The only differences are a more distinct dipole

273 structure between the Canada Basin and Eurasian Basin, and positive EOF loading (instead of
274 negative in the first mode of series 2) over much of the Nordic seas that appears in the first
275 mode of series 2. As the Nordic seas region is the pathway of Atlantic waters in the Arctic
276 Basin (Karcher et al., 2007), we assume that the change of sign of EOF values is associated
277 with increased temperature and salinity of Atlantic water inflow and subsequent salinification
278 of the Eurasian Basin (Polyakov et al., 2010; Beszczynska-Möller et al., 2012). Thus, the modes
279 obtained by decomposition in series 1 cannot take into account the essential features of the
280 distribution of surface-layer salinity fields associated with the salinification of the Eurasian
281 Basin. Therefore, for further analysis we used the principal components and modes obtained
282 upon decomposition in series 2 (Figure 2).

283 As a point of comparison for these EOFs, Appendix Figure A3 presents a similar EOF
284 analysis using model output from the PIOMAS. The spatial pattern of PIOMAS mean salinity
285 (Figure A3a) reasonably resembles the pattern shown for our data in Figure 2a. EOFs of
286 PIOMAS salinity after detrending (Figure A3b-d) repeat the main features of corresponding
287 results in Figure 2b-d, despite incomplete overlap over the analysis periods. In particular, for
288 both data sets, the leading EOF for salinity features a prominent dipole between the Canada
289 Basin and Eurasian Basin (Figures 2b and A3b). However, the leading EOF of PIOMAS
290 salinity has a more patchy structure. In particular, there are negative centers of action situated
291 along the Siberian shelf break, along with freshened areas (Figure A3a) that are not as clearly
292 pronounced in the AARI salinity data (Figure 2a). The second EOF of salinity features a
293 negative center of action elongated along the Lomonosov Ridge surrounded by positive loading
294 strongest along Siberian shelf (Figures 2c and A3c). Less agreement is seen for the third EOF
295 (Figures 2d and A3d), which is perhaps unsurprising in moving toward modes accounting for
296 less variance.

297 **3.2. The linear regression equation for the principal components**

298 We present here a statistical model of inter-annual variability of Arctic Ocean surface-
299 layer salinity. This research builds on already established approaches used by Pokroivsky and
300 Timokhov (2002), specifically their reconstruction of salinity fields applying modified EOF
301 methods.

302 We suggest some additions to improve the ideas presented in previous research. For
303 example, the analysis presented is based on a dataset updated for the period 2007-2012, which
304 is important for understanding the physical processes during the dramatic recent changes in
305 Arctic sea ice. The area under consideration was extended and includes the Nordic seas and
306 part of the Siberian shelf with depths of more than 50 m. Also, in contrast to our previously
307 published research (Timokhov et al., 2012), we do not use the previous values of the principal
308 components (history) as predictors for linear regression, which simplifies the physical
309 interpretation of the equations obtained.

310 A set of external factors having the most correlation with salinity values have been
311 defined based on the results of correlation analysis. As a result of linear regression analysis we
312 obtained empirical equations for the first three PCs (see Table A2 in Appendix). The structure
313 of these equations can be explained through the sets of factors that simulate the effects of both
314 atmospheric and hydrological processes.

315 Thus, the predictors used can be divided into two groups. The first group includes
316 atmospheric circulation indices and reflects the influence of atmospheric processes. The second
317 group corresponds to hydrological processes: river runoff into Arctic seas, inflows through the
318 Bering Strait and the Faeroe-Shetland Strait, which were characterized by the PDO and AMO
319 indices, and the areas of open water in the Arctic seas in September. Predictors were included
320 in the equations with different time shifts (lags). The value of the time shift was 1–10 years and
321 was chosen to maximize correlations of predictors with the PCs as noted above.

322 The contribution of each group to the explained variance in PC₁ through PC₃ can be
323 calculated based on the magnitude and sign of the regression coefficients of corresponding
324 predictors included in that particular group. In this case, hydrological processes have a
325 dominant contribution to the explained variance of all PCs. Atmospheric factors (i.e., AO and
326 AD) contribute from 14 to 39%.

327

328 **4. Discussion and Summary**

329 The first mode of the surface-layer salinity decomposition (EOF₁) displays an out-of-
330 phase relationship between salinity anomalies in the Canada and Eurasian Basins (which
331 includes the Nansen and Amundsen Basins) and Makarov Basin (Figure 2b).

332 In the late 1980s, as a consequence of surface air temperature rising, the atmospheric
333 circulation regime in the Arctic began to change (Steele and Boyd, 1998; Proshutinsky et al.,
334 2009; Morison et al., 2012). Degradation of the Arctic anticyclone, shifting of the pressure
335 pattern counterclockwise from the 1979-1992 pattern (Morison et al., 2000), and strengthening
336 of the dipole pressure pattern (Overland et al., 2008) were observed. According to Wang et al.
337 (2009), large values of the AD indices (higher than 0.6 standard deviation) could be a primary
338 reason for the historical record lows of sea ice extent in the summers of 1995, 1999, 2002, 2005
339 and 2007. In addition, in the late 1980s the inflow of warm and highly saline Atlantic water
340 into the Arctic Basin increased (Morison et al., 2000; Polyakov et al., 2010). Observed shoaling
341 of the Atlantic water upper boundary, together with a decrease of static stability in the halocline
342 layer, led to an increase in upper layer temperature and salinity in the Eurasian Basin (Polyakov
343 et al., 2010). At the beginning of this century, the heat flux through the Bering Strait to the
344 Chukchi Sea increased (Woodgate et al., 2010). Comparatively warm and fresh (salinity range
345 31<S<32) summer Pacific waters, due to their low density, were able to inject heat close to the

346 ocean surface (Stigebrandt, 1984) and enhance ice melting in the Canada Basin (Shimada et
347 al., 2006) which led to decreasing surface-layer salinity in this region.

348 These observations allow us to suggest that salinity differences between the Canada
349 Basin and Eurasian Basin, which became more pronounced in recent years (Figure 1), are the
350 consequence of these processes. Our suggestion is supported by the regression equation for
351 PC_1 (Table A2) from which we see that PC_1 is a function of AMO, PDO, open water area in
352 the East Siberian and Chukchi seas (that can be considered as an indirect indicator of fresh
353 water inflow from these seas to the Arctic) and summer AO index. The time lags must be
354 related with the time that it takes for Atlantic and Pacific waters to reach the Arctic Basins and
355 become involved in associated circulation.

356 According to Karcher et al. (2002), travel time for the propagation of anomalies in AW
357 is 5-10 years from the Nordic Seas to the Eurasian Basin. Bourgain and Gascard (2012)
358 revealed that the warm signal from the Bering Strait propagated in the interior of the Canada
359 Basin during 4-5 years. The travel times for the Siberian river water from the river mouths to
360 the shelf edge are estimated to be 2-5 years (Schlosser et al., 1994; Karcher et al., 2002). These
361 time periods are in good agreement with time lags of the statistical model predictors (Table
362 A2).

363 EOF_2 exhibits opposite polarity of salinity anomalies in the central Arctic Ocean and
364 near-slope areas (Figure 2c). Spectral analysis of the associated PC_2 revealed a 9-year cycle
365 (periodogram is not shown here), which we associate with shifts between cyclonic and
366 anticyclonic circulation regimes (Proshutinsky and Johnson, 1997; Rigor et al., 2002). The
367 regression equation for PC_2 demonstrates its dependence on the summer AO and AD indices.
368 Thus, during an anti-cyclonic regime of atmospheric circulation, fresh surface waters tend to
369 flow to the center of the Arctic basin and negative salinity anomalies form there. At the same
370 time, along the slopes there is upwelling of Atlantic waters and positive salinity anomalies

371 occur (Proshutinsky and Johnson, 1997). During a cyclonic circulation regime, reversed
 372 momentum forcing should likewise produce positive salinity anomalies in the central Arctic
 373 and negative salinity anomalies along the slopes.

374 The contribution of each predictor in the variability of a particular PC was evaluated
 375 as:

$$376 \quad I = \frac{\sigma_i \cdot \alpha}{\sum(\sigma_i \cdot \alpha)} \cdot 100\% , \quad (9)$$

377 where σ_i is the standard deviation of the predictor and α is the regression coefficient of the
 378 predictor. According to this formula, contributions of the predictors for PC₂ (Table A2) were
 379 calculated. PDO and river runoff from the Laptev, East Siberian and Chukchi Seas make the
 380 largest contribution to the variability of PC₂ (33.8 and 26.9 %, respectively) with slightly
 381 weaker effects from AO and AD (20.5 and 18.9 %).

382 EOF₃ is represented by a field with multicore structure (Figure 2d). The positive centers
 383 of action spread from the Beaufort Sea over the North Pole to the Kara Sea and are surrounded
 384 by negative centers of action. This kind of distribution is associated with an Arctic Dipole (Wu
 385 et al., 2006). The winter AD index accounts for approximately 22% of the variability of PC₃.
 386 The most distinct negative cores are located along the shelf of the Laptev and Chukchi Seas
 387 and also near Greenland. In our statistical model, associated variations are accounted for by
 388 river runoff from the Laptev, East Siberian and Chukchi Seas, the PDO index, and the AMO
 389 index, which account for 20, 25.8 and 32.4% of the variability of PC₃, respectively (Table A2).

390 All predictors included in the regression equations (with particular time lags and
 391 averaging periods) are statistically independent, i.e. they are not significantly correlated with
 392 each other, except for AMO(-10) and PDO(-3). These indices have a slight positive correlation
 393 ($R = 0.33$), but this is not a concern because they have different regions of influence and are
 394 associated with different proxies.

395 Time series of PC₁₋₃ show a mixture of interannual and quasidecadal oscillations
396 (Figure 3). Based on the configurations of the EOFs (Figure 2), the regression equations (Table
397 A2) and results of the spectral analysis of the PCs, we may assume that large-scale surface
398 layer salinity anomalies (with periods longer than 20 years) are the result of water exchange
399 effects. The shorter-period (8-9 years) variations appear to be determined by atmospheric
400 circulation processes. Also, interannual variations occur due to interannual variability of both
401 atmospheric and hydrological processes.

402 The derived equations in the Appendix (Table A2) describe the first three principal
403 components for the period 1950-2012. Calculated with these equations, the modeled PCs agree
404 well with the values of the PCs directly derived from the decomposition of salinity fields via
405 EOF analysis (Figure 3).

406 Theoretically, the salinity fields for 1994-2006 can be reconstructed using this statistical
407 model. We noted above that this period had gaps in observational data. The salinity fields of
408 1995, 2000, and 2005 were chosen for reconstruction to demonstrate the capabilities of the
409 statistical model. The results were compared with PIOMAS model data. Though reconstructed
410 fields have high significant correlations with PIOMAS fields (correlation coefficients are 0.84,
411 0.88 and 0.81), in the Amerasian Basin they show lower salinity values than PIOMAS data.
412 Differences in this region may reach 2 psu. In the Eurasian Basin, specially over the
413 Lomonosov Ridge, reconstructed salinity values are higher than PIOMAS data with differences
414 of up to 1.5 psu (for 2005) (Figure 4).

415 Also, we applied our statistical model to the reconstruction of salinity fields for 2013-
416 2014, extending beyond the data record in order to develop a retrospective forecast (sometimes
417 referred to as a hindcast). As a result, we obtained salinity fields that correspond to the trends
418 observed in recent years. This preserved the freshening in the Canada Basin as well as
419 salinification of the surface layer over the Lomonosov Ridge (compared with average surface-

420 layer salinity for 1961-1990) (Figure 5). According to our modeled values for 2013-2014,
 421 freshened water from the Beaufort Gyre should have moved westward along the Canadian
 422 Continental Slope in 2013. Also there are negative salinity anomalies observed in the Arctic
 423 seas along the Siberian shelf. These processes were able to freshen the Eurasian Basin slightly
 424 so that in 2014 positive salinity anomalies over the Lomonosov Ridge were lower than in 2013.
 425 To demonstrate the quality of the forecast, we compared the salinity field for 2013 with the
 426 corresponding gridded field of observational data and PIOMAS data (Figure 5). As we were
 427 not able to find enough data in winter 2014 to produce a reliable gridded field, comparison for
 428 this year was not conducted. In both cases it is seen that the reconstructed values are lower in
 429 the Canadian Basin and higher in the Eurasian Basin. However, our results are closer to the
 430 observational data than to the PIOMAS data, as differences in the first case are not larger than
 431 0.7 psu (Figure 5) and in the second case they are as large as 2.5 psu.

432 This method of salinity reconstruction may suffer from inaccuracies due to the higher-
 433 frequency variability of the calculated PCs. The model may not reliably generate principal
 434 components for short-term time series, although the trend in variability of all three PCs is
 435 reproduced correctly. Therefore, the model can be used for tracking long-term processes of the
 436 structure transformation of salinity fields.

437 Validation of the model was carried out by calculating an error of reconstruction for the
 438 surface-layer salinity fields. The difference between the actual and reconstructed salinity fields
 439 (ε) was determined as a percentage by the following formula:

$$440 \quad \varepsilon = \left(\sigma(S_f - S_c) / \sigma(S_f) \right) \cdot 100\% \quad (10)$$

441 where σ is the standard deviation, S_f is the actual salinity, and S_c is the calculated salinity.

442 Twelve surface-layer salinity fields from the time series under consideration (fields for
 443 the years 1950, 1955, 1960, 1965, 1970, 1975, 1980, 1985, 1990, 2007, 2009 and 2011) were
 444 reconstructed, using modeled values of the PCs. The years were chosen at approximately equal

445 intervals in order to reflect the different stages of the salinity field evolution through all
446 decades. The average error of reconstruction for the chosen fields was 18.4%. As the first three
447 EOF modes describe 61% of the variability of the initial fields, the error obtained is less than
448 the variance not covered by the first three EOFs. Thus we have a system of regression equations
449 (statistical model) that may skillfully reproduce long-term salinity anomalies. The rest of the
450 surface-layer salinity variance captured by higher-order EOFs (approximately 39%) is likely
451 explained by short-term and probably local processes such as ice formation and cascading in
452 polynya regions (Ivanov and Watanabe, 2013), deep convection, or mixing with the Atlantic
453 water upper boundary (Ivanov et al., 2012).

454 Thus we have identified various patterns in Arctic Ocean surface-layer salinity fields
455 using a reliable statistical model. In addition, we have found anomalies in the salinity fields
456 which have occurred in the past, and conclude that more than 60% of surface-layer salinity
457 variability is related to long-term processes and nearly 40% is due to short-term and local
458 processes. Our findings again raise questions about nonlinearities in global ocean circulation,
459 particularly in the Arctic Ocean, which is strongly connected with Earth's climate system. In
460 the future, information obtained about these anomalies may be helpful in determining whether
461 Arctic Ocean salinity, and related oceanographic phenomena, have reached a critical threshold.

462 **Acknowledgments**

463 The authors thank the following data providers. The detailed algorithm of the salinity
464 data gridding procedure is available at the AARI web-site:
465 [http://www.aari.ru/resources/a0013_17/kara/Atlas_Kara_Sea_Winter/text/tehnik_report.htm#](http://www.aari.ru/resources/a0013_17/kara/Atlas_Kara_Sea_Winter/text/tehnik_report.htm#p2)
466 [p2](http://www.aari.ru/resources/a0013_17/kara/Atlas_Kara_Sea_Winter/text/tehnik_report.htm#p2). Indices of atmospheric circulation are available at NOAA's Data Base. The area of ice-free
467 surface in the Arctic Ocean was calculated from data cited at
468 <https://www.aari.ru/projects/ECIMO/index.php?im=100>. River runoff data were obtained from

469 the Joint US-Russian Atlas of the Arctic Ocean and Arctic RIMS Data Server. We thank M.
470 Janout for providing AD indices north of 60°N.

471 The authors are grateful for financial support from the Otto Schmidt Laboratory for
472 Polar and Marine Research (Grant OSL-13-05), and from the Russian Foundation for Basic
473 Research (Grants 14-01-31053_mol_a; 16-34-00733_mol_a; 16-31-60070_mol_a_dk).
474 Finally, we gratefully acknowledge support from the Division of Mathematical Sciences and
475 the Division of Polar Programs at the U.S. National Science Foundation (NSF) through Grants
476 ARC-0934721, DMS-0940249, and DMS-1413454. We are also grateful for support from the
477 Office of Naval Research (ONR) through Grant N00014-13-10291. We would like to thank the
478 NSF Math Climate Research Network (MCRN) as well for their support of this work. We thank
479 N. Lebedev and V. Karpy for help with data processing. In preparing this text, we have
480 benefited from discussions with Jessica R. Houf.

481 **References**

- 482 Beszczynska-Möller, A., Fahrbach, E., Schauer, U., Hansen, E., 2012. Variability in Atlantic
483 water temperature and transport at the entrance to the Arctic Ocean, 1997–2010, *ICES*
484 *Journal of Marine Science*, Volume 69, Issue 5, pp. 852–863,
485 doi:10.1093/icesjms/fss056
- 486 Borzelli, G., Ligi, R., 1998. Empirical Orthogonal Function Analysis of SST Image Series: a
487 Physical Interpretation. *J. Atmos. Oceanic Technol.* 16, 682–690.
- 488 Bourgain, P. and Gascard, J.C., 2012. The Atlantic and summer Pacific waters variability in
489 the Arctic Ocean from 1997 to 2008. *Geophys. Res. Lett.*, 39, L05603,
490 doi:10.1029/2012GL051045
- 491 Carmack, E.C., 2000. The Arctic Ocean's freshwater budget: sources, storage and export, in:
492 Lewis, E.L., Jones, E.P., Lemke, P., Prowse, T.D., Wadhams, P. (Eds), *The Freshwater*
493 *Budget of the Arctic Ocean. Kluwer Academic Publishers*, pp. 91–126.

- 494 Cronin, M. F., Sprintall, J., 2001. Wind and buoyancy-forced upper ocean, in: Steele, J.,
495 Thorpe, S., Turekian, K. (Eds.), *Encyclopedia of Ocean Sciences*, Vol. 6. Academic
496 Press, pp. 3219-3227
- 497 Dickson, B., 1999. Oceanography: All change in the Arctic. *Nature*, 397(6718), 389-391.
- 498 Dima, M., Lohmann, G., 2007. A Hemispheric Mechanism for the Atlantic Multidecadal
499 Oscillation. *J. Climate*, 20, 2706-2719. doi: 10.1175/JCLI4174.1
- 500 Enfield, D.B., Mestas-Nunez, A.M., Trimble, P.J., 2001. The Atlantic Multidecadal
501 Oscillation and its relationship to rainfall and river flows in the continental U.S.
502 *Geophys. Res. Lett.* 28, 2077-2080.
- 503 Gelderloos, R., Straneo, F. and Katsman, C.A., 2012. Mechanisms behind the Temporary
504 Shutdown of Deep Convection in the Labrador Sea: Lessons from the Great Salinity
505 Anomaly Years 1968–71. *J. Climate*, 25, 6743–6755, doi.org:10.1175/JCLI-D-11-
506 00549.1
- 507 Ivanov, V., Alexseev, V., Repina, I., Koldunov, N. and Smirnov, A., 2012. Tracing Atlantic
508 Waters Signature in the Arctic sea ice cover East of Svalbard. *Advances in Meteorology*,
509 doi:10.1155/2012/201818
- 510 Ivanov, V. and Watanabe, E., 2013. Does Arctic sea ice reduction foster shelf-basin exchange?
511 *Ecological Applications*, 23(8), 1765-1777.
- 512 Haak, H., Jungclaus, J., Mikolajewicz, U. and Latif M., 2003. Formation and propagation of
513 great salinity anomalies. *Geophys. Res. Lett.*, 30, 1473, doi:10.1029/2003GL017065.9
- 514 Hannachi, A., Jolliffe, I.T., Stephenson, D.B., 2007. Empirical orthogonal functions
515 and related techniques in atmospheric science: a review. *Int. J. Climatol.* 27, 1119-
516 1152. doi:10.1002/joc.1499
- 517 Hall, A., Stouffer, R. J., 2001. An abrupt climate event in a coupled ocean-atmosphere
518 simulation without external forcing. *Nature*, 409(6817), 171.

- 519 Hill, T., Lewicki, P., 2007. Statistics: Methods and Applications. *StatSoft*, Tulsa, OK.
- 520 Jackson, J.M., Williams, W.J., Carmack, E.C., 2012. Winter sea-ice melt in the Canada Basin,
521 Arctic Ocean. *Geophys. Res. Lett.* 39, L03603, doi:10.1029/2011GL050219.
- 522 Jahn, A., Aksenov, Y., de Cuevas, B. A., de Steur, L., Häkkinen, S., Hansen, E., Herbaut, C.,
523 Houssais, M.-N., Karcher, M., Kauker, F., Lique, C., Nguyen, A., Pemberton, P.,
524 Worthen, D., Zhang, J., 2012. Arctic Ocean freshwater: How robust are model
525 simulations. *J. Geophys. Res. Oceans*, 117(C8), 2156-2202, doi:
526 10.1029/2012JC007907.
- 527 Karcher, M., Oberhuber, J. M., 2002. Pathways and modification of the upper and intermediate
528 waters of the Arctic Ocean. *J. Geophys. Res.*, 107 (C6), doi:10.1029/2000JC000530.
- 529 Karcher, M., Kauker, F., Gerdes, R., Hunke, E. and Zhang, J., 2007. On the dynamics of
530 Atlantic Water circulation in the Arctic Ocean. *J. Geophys. Res.*, 112, C04S02,
531 doi:10.1029/2006JC003630.
- 532 Kistler, R., Kalnay, E., Collins, W., Saha, S., White, G., Woollen, J., Chelliah, M., Ebisuzaki,
533 W., Kanamitsu, M., Kousky, V., van den Dool, H., Jenne, R., Fiorino, M., 2001. The
534 NCEP-NCAR 50-Year Reanalysis: Monthly Means CD-ROM and Documentation.
535 *Bull. Amer. Meteor. Soc.* 82, 247-268.
- 536 Komuro, Y., 2014. The Impact of Surface Mixing on the Arctic River Water Distribution and
537 Stratification in a Global Ice–Ocean Model. *J. Climate*, 27, 4359–4370.
538 doi:10.1175/JCLI-D-13-00090.1
- 539 Korhonen, M., Rudels, B., Marnela, M., Wisotzki, A., Zhao, J., 2013. Time and space
540 variability of freshwater content, heat content and seasonal ice melt in the Arctic Ocean
541 from 1991 to 2011. *Ocean Science*, 9 (6), 1015-1055.

- 542 Lebedev, N.V., Karpy, V.Yu., Pokrovsky, O.M., Sokolov, V.T., Timokhov, L.A., 2008.
543 Specialized data base for temperature and salinity of the Arctic Basin and marginal seas
544 in winter (in Russian). *Trudy AANII*, 448, 5-17.
- 545 Lique, C., Treguier A., Scheinert M., Penduff T., 2009. A model-based study of ice and
546 freshwater transport variability along both sides of Greenland. *Clim. Dyn.*, 33, 685–
547 705, doi:10.1007/s0038200805107.
- 548 Lindsay, R.W., Zhang, J., 2006. Assimilation of ice concentration in an ice-ocean model. *J.*
549 *Atmos. Ocean. Tech.*, 23, 742-749.
- 550 Macdonald, R.W., Harner, T., Fyfe J., 2005. Recent climate change in the Arctic and its impact
551 on contaminant pathways and interpretation of temporal trend data. *In Science of The*
552 *Total Environment*, Vol. 342, Issues 1–3, pp. 5-86, ISSN 0048-9697,
553 doi:10.1016/j.scitotenv.2004.12.059.
- 554 Morison, J. and Smith J. D., 1981. Seasonal variations in the upper Arctic Ocean as observed
555 at T-3. *Geophys. Res. Lett.*, 8(7), 753–756, doi:10.1029/GL008i007p00753.
- 556 Morison, J., Aagaard, K. and Steele, M., 2000. Recent Environmental Changes in the Arctic: a
557 review. *Arctic*, vol. 53, NO. 4, 359-371.
- 558 Morison, J., Kwok, R., Peralta-Ferriz, C., Alkire, M., Rigor, I., Andersen, R., Steele, M., 2012.
559 Changing Arctic Ocean freshwater pathways. *Nature*, 481, 66-70, doi:
560 10.1038/nature10705.
- 561 Nguyen, A. T., D. Menemenlis, R. Kwok, 2009. Improved modeling of the Arctic halocline
562 with a subgrid-scale brine rejection parameterization. *J. Geophys. Res.*, 114, C11014,
563 doi:10.1029/2008JC005121.
- 564 North, G.R., Bell, T.L., Cahalan, R.F. and Moeng, F.J., 1982. Sampling errors in the estimation
565 of empirical orthogonal functions. *Monthly Weather Review*, 10, 699-706.

- 566 Overland, J.E., Wang, M., 2010. Large-scale atmospheric circulation changes are associated
567 with the recent loss of Arctic sea ice. *Tellus*, 62A, 1-9.
- 568 Pokrovsky, O.M., Timokhov, L.A., 2002. The Reconstruction of the Winter Fields of the Water
569 Temperature and Salinity in the Arctic Ocean. *Oceanology*, 42, 822-830.
- 570 Polyakov, I.V., V.A. Alexeev, G.I. Belchansky, I.A. Dmitrenko, V.V. Ivanov, S.A. Kirillov,
571 A.A. Korablev, M. Steele, L.A. Timokhov, and I. Yashayaev, 2008. Arctic Ocean
572 Freshwater Changes over the Past 100 Years and Their Causes. *J. Climate*, 21, 364–
573 384, doi:10.1175/2007JCLI1748.1
- 574 Polyakov, I.V., Timokhov, L.A., Alexeev, V.A., Bacon, S., Dmitrenko, I.A., Fortier, L., Frolov,
575 I.E., Gascard, J.-C., Hansen, E., Ivanov, V.V., Laxon, S., Mauritzen, C., Perovich, D.,
576 Shimada, K., Simmons, H.L., Sokolov, V.T., Steele, M., Toole, J., 2010. Arctic Ocean
577 warming contributes to reduced Polar Ice Cap. *J. Phys. Oceanogr.* 40, 2743-2756.
- 578 Proshutinsky, A.Y., Krishfield, R., Timmermans, M.-L., Toole, J., Carmack, E., McLaughlin,
579 F., Williams, W.J., Zimmermann, S., Itoh, M., Shimada, K., 2009. Beaufort Gyre
580 freshwater reservoir: State and variability from observations. *J. of Geophys. Res.* 114,
581 doi: 10.1029/2008JC005104.
- 582 Proshutinsky, A.Y., Johnson, M.A., 1997. Two circulation regimes of the wind-driven Arctic
583 Ocean. *J. of Geophys. Res.* 102, 12493-12514.
- 584 Rabe, B., Karcher, M., Schauer, U., Toole, J.M., Krishfield, R.A., Pisarev, S., Kauker, F.,
585 Gerdes, R., Kikuchi, T., 2011. An assessment of Arctic Ocean freshwater content
586 changes from the 1990s to the 2006–2008 period. *Deep-Sea Res. Part. I*, 58, 173–185.
- 587 Rigor I.G., Wallace J.M., Colony R.L., 2002. Response of sea ice to the Arctic Oscillation. *J.*
588 *Climate*, 15, 2648-2663.
- 589 Rudels, B., Anderson, L.G., Jones, E.P., 1996. Formation and evolution of the surface mixed
590 layer and halocline of the Arctic Ocean. *J. of Geophys. Res.* 101, 8807-8821.

- 591 Schlosser, P., Bauch, D., Fairbanks, R. and G. Bönisch, 1994. Arctic river runoff: mean
592 residence time on the shelves and in the halocline, *Deep Sea Res., Part I*, 41, 1053–
593 1068.
- 594 Shimada K., Kamoshida T., Itoh M., Nishino S., Carmack E., McLaughlin F., Zimmermann S.
595 and Proshutinsky A., 2006. Pacific Ocean inflow: influence on catastrophic reduction
596 of sea ice cover in the Arctic Ocean. *Geophys. Res. Lett.*, 33, L08605, doi:
597 10.1029/2005GL025624.
- 598 Steele, M., Boyd, T., 1998. Retreat of the cold halocline layer in the Arctic Ocean. *J. of*
599 *Geophys. Res.* 103, doi: 10.1029/98JC00580.
- 600 Steele, M., W. Ermold, G. Holloway, S. Häkkinen, D. M. Holland, M. Karcher, F. Kauker, W.
601 Maslowski, N. Steiner, J. Zhang, 2001. Adrift in the Beaufort Gyre: A model
602 ntercomparison. *Geophys. Res. Lett.*, 28, 2835–2838.
- 603 Stigebrandt, A., 1984. The North Pacific: A Global-Scale Estuary. *J. Phys. Oceanogr.*, 14, 462-
604 470.
- 605 Thompson, D.W.J. and Wallace J.M., 1998. Observed linkages between Eurasian surface air
606 temperature, the North Atlantic Oscillation, Arctic Sea-level pressure and the
607 stratospheric polar vortex. *Geophys. Res. Lett.*, 25, 1297-1300, 1998.
- 608 Timmermans, M.-L., Proshutinsky, A., Krishfield, R.A., Perovich, D.K., Richter-Menge,
609 J.A., Stanton, T.P., Toole, J.M., 2011. Surface freshening in the Arctic Ocean's
610 Eurasian Basin: an apparent consequence of recent change in the wind-driven
611 circulation. *J. of Geophys. Res.* 116, doi:10.1029/2011JC006975.
- 612 Timokhov, L.A., Chernyavskaya, E.A., Nikiforov, E.G., Polyakov, I.V., Karpy, V. Yu., 2012.
613 Statistical model of inter-annual variability of the Arctic Ocean surface layer salinity in
614 winter (in Russian). *Probl. Arkt. i Antarkt.* 91, 89-102.

- 615 Timokhov, L.A., Tanis, F., 1997. Environmental Working Group Joint U.S.-Russian Atlas of
616 the Arctic Ocean. *National Snow and Ice Data Center*, Boulder, Colorado, USA,
617 <http://dx.doi.org/10.7265/N5H12ZX4>.
- 618 Toole, J. M., M.-L. Timmermans, D. K. Perovich, R. A. Krishfield, A. Proshutinsky, and J. A.
619 Richter-Menge, 2010. Influences of the ocean surface mixed layer and thermohaline
620 stratification on Arctic sea ice in the central Canada Basin. *J. Geophys. Res.*, 115,
621 C10018, doi:10.1029/2009JC005660.
- 622 Trenberth, K.E. and Hurrell, J.W. 1994: Decadal atmosphere-ocean variations in the Pacific.
623 *Clim. Dyn.* 9, 303-319.
- 624 Treshnikov, A.F., 1959. Arctic Ocean surface waters (in Russian). *Probl. Arkt.* 7, 5-14.
- 625 Walin G, 1985. The thermohaline circulation and the control of ice ages. *Palaeogeography,*
626 *Palaeoclimatology, Palaeoecology*, Vol. 50, Issues 2–3, pp. 323-332, ISSN 0031-0182,
627 doi:10.1016/0031-0182(85)90075-6.
- 628 Wang, J., Zhang, J., Watanabe, E., Ikeda, M., Mizobata, K., Walsh, J. E., Bai, X., Wu, B.,
629 2009. Is the Dipole Anomaly a major driver to record lows in Arctic summer sea ice
630 extent? *Geophys. Res. Lett.* 36, L05706, doi 10.1029/08GL036706.
- 631 Weyl P.K., 1968. The Role of the Oceans in Climatic Change: A Theory of the Ice Ages. In:
632 Mitchell J.M. (eds) Causes of Climatic Change. *Meteorological Monographs*, vol 8.
633 American Meteorological Society, Boston, MA
- 634 Woodgate, R.A., Weingartner, T., Lindsay, R., 2010. The 2007 Bering Strait oceanic heat flux
635 and anomalous Arctic sea-ice retreat. *Geophys. Res. Lett.* 37, L01602, doi:
636 10.1029/2009GL041621.
- 637 Wu, B., Wang, J., Walsh, J.E., 2006. Dipole Anomaly in the Winter Arctic Atmosphere and
638 Its Association with Sea Ice Motion. *J. of Climate.* 19, 210–225.

- 639 Zhang, J., Rothrock, D.A., 2003. Modeling global sea ice with a thickness and enthalpy
640 distribution model in generalized curvilinear coordinates. *Mon. Wea. Rev.* 131(5),
641 681-697.
- 642 Zhang, J., Woodgate, R., Moritz, R., 2010. Sea Ice Response to Atmospheric and Oceanic
643 Forcing in the Bering Sea. *J. Phys. Oceanogr.*, 40, 1729-1747.
644 doi:10.1175/2010JPO4323.1
645

646 Table 1. Predictors used for the approximation of PCs.

Physical processes and its notation	Physical value	Description	Data sources (references and the web sources)
Arctic oscillation index (AO)	First EOF-mode of Sea-level pressure north of 60N latitude	<p>When the AO index is positive, surface pressure is low in the polar region.</p> <p>When the AO index is negative, there tends to be high pressure in the polar region.</p>	<p><i>Thompson and Wallace (1998).</i></p> <p>NOAA Center for Weather and Climate Prediction (NCWCP)</p> <p>http://www.esrl.noaa.gov/psd/data/gridded/</p>
Arctic Dipole Anomaly index (AD)	Second EOF-mode of Sea-level pressure north of 60N latitude	<p>When the AD index is positive, sea-level pressure has a positive anomaly over the Canadian Archipelago and a negative anomaly over the Barents Sea.</p> <p>When the AD index is negative, SLP anomalies show an opposite scenario, with the center of negative SLP anomalies over the Nordic seas. (Wu et al., 2006; Wang et al., 2009; Overland & Wang, 2010).</p>	<p><i>Overland and Wang (2010).</i></p> <p>NOAA Center for Weather and Climate Prediction (NCWCP)</p> <p>http://www.esrl.noaa.gov/psd/data/gridded/</p>

Atlantic Multi decadal oscillation index (AMO)	Variations of sea surface temperature in the North Atlantic Ocean	Index has cool and warm phases that may last for 20-40 years at a time and a difference of about 0.5°C. It reflects changes of sea surface temperature in the Atlantic Ocean between the equator and Greenland. It was used as a substitute for processes of water exchange with the Atlantic Ocean.	<i>Enfield et al.</i> (2001). ESRL Physical Sciences Division (PSD) http://www.esrl.noaa.gov/psd/data/timeseries/AMO/
The Pacific Decadal Oscillation index (PDO)	North Pacific sea surface temperature variability	When the PDO index is positive, the west Pacific becomes cool and part of the eastern ocean warms. When the PDO index is negative, the opposite pattern occurs. It shifts phases on at least the inter-decadal time scale, usually about 20 to 30 years.	<i>Trenberth and Hurrell</i> (1994). Joint Institute for the Study of the Atmosphere and Ocean (JISAO) http://jisao.washington.edu/pdo/
River runoff (RIV)	Water flows	Average annual runoff of the main Siberian rivers. It was used as total runoff in the Kara Sea (K), Laptev Sea (L), East-Siberian Sea (E) and Chukchi Sea (C).	<i>Timokhov and Tanis</i> (1997). Joint US-Russian Atlas of the Arctic Ocean. http://rims.unh.edu/data/station/list.cgi?col=4

Area of open water in Arctic seas (OW)	Area	Total ice-free area in the Kara Sea (K), Laptev Sea (L), East-Siberian Sea (E) and Chukchi Sea (C) in September.	Russian Arctic and Antarctic Research Institute (AARI) http://www.aari.ru/projects/ECIMO/index.php?im=100
--	------	--	--

647

648

649

650

651

652

653

654

655

656 **Figure Caption List:**

657 Figure 1. Temporal changes in salinity averaged over the depth range 5-50 m. Dashed curves
658 show salinities from PIOMAS data. Grids with spatial resolution 200x200 km were obtained
659 as the result of interpolation and reconstruction (see section 2.2) of bottled and CTD data.

660

661 Figure 2. The average salinity field (a) and first three modes of the average salinity field
662 decomposition for the layer 5-50 m: (b), (c), (d) - 1st, 2nd and 3rd modes, respectively, for the
663 period 1950-1993 and 2007-2012.

664

665 Figure 3. The actual (black line) principal components and calculated principal components
666 (red dashed line) with the help of the equations of linear regression. Correlation coefficients
667 between the calculated time series of PCs and actual PCs are: $r(PC_1)=0.88$; $r(PC_2)=0.73$;
668 $r(PC_3)=0.55$.

669

670 Figure 4. Maps of differences of salinity fields reconstructed with the statistical model and
671 those from PIOMAS data.

672

673 Figure 5. Reconstructed salinity fields for the layer 5-50 m in 2013 (a) and 2014 (b); actual
674 salinity field for the layer 5-50 m in 2013 (c) (from AARI data), difference between actual
675 salinity field and reconstructed one for 2013 (d); PIOMAS salinity field for 2013 (e) and
676 difference between PIOMAS salinity field and reconstructed one for 2013(f).

677

678 Figure A1. Observation density. Color bar indicates the last number of the year in each decade.
679 The total number of observations in the 1950s – 428, 1960s – 751, 1970s – 3837, 1980s – 4374,
680 1990s – 556, 2000s – 14691.

681 Figure A2. Schematic diagram of the conceptual statistical model.

682

683 Figure A3. Same as Figure 2, but for salinity averaged annually over the upper 50 m of

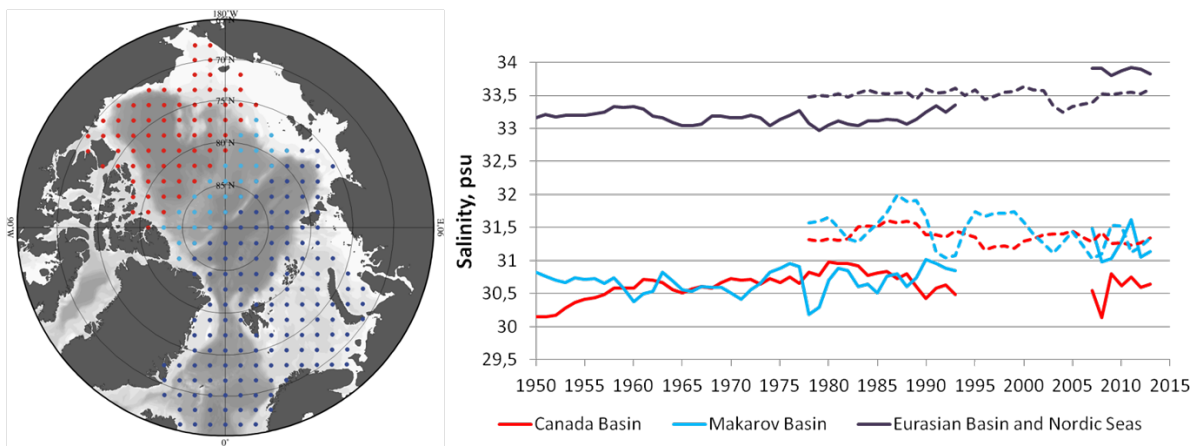
684 PIOMAS data for 1978-2012.

685

686 Figure A4. Variance maps of surface layer salinity for the 1978-2012 period: a) – AARI data

687 base, b) – PIOMAS data.

688



689

690 Figure 1. Temporal changes in salinity averaged over the depth range 5-50 m. Dashed curves

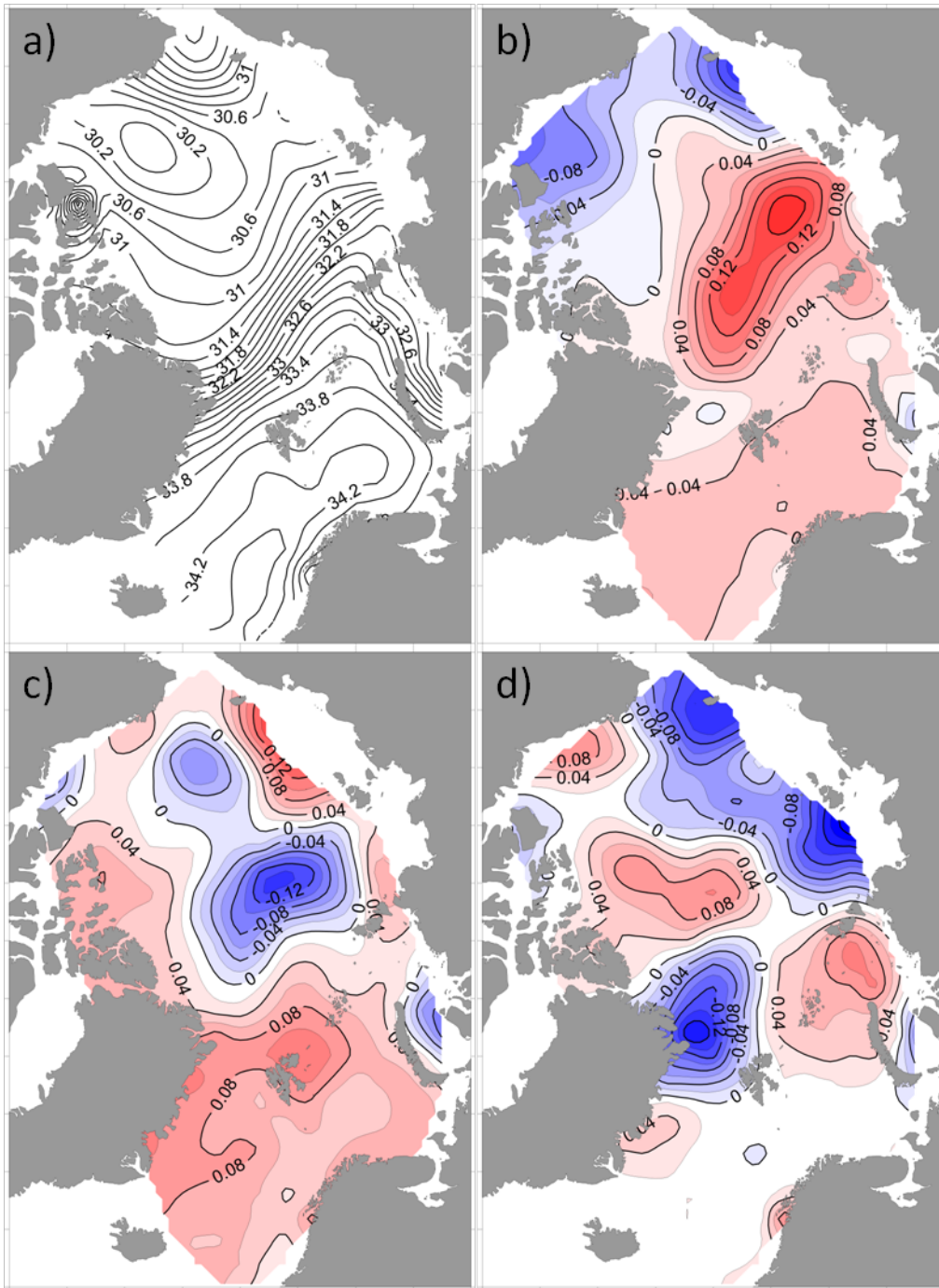
691 show salinities from PIOMAS data. Grids with spatial resolution 200x200km were obtained as

692 the result of interpolation and reconstruction (see Section 2.2) of bottled and CTD data.

693

694

695

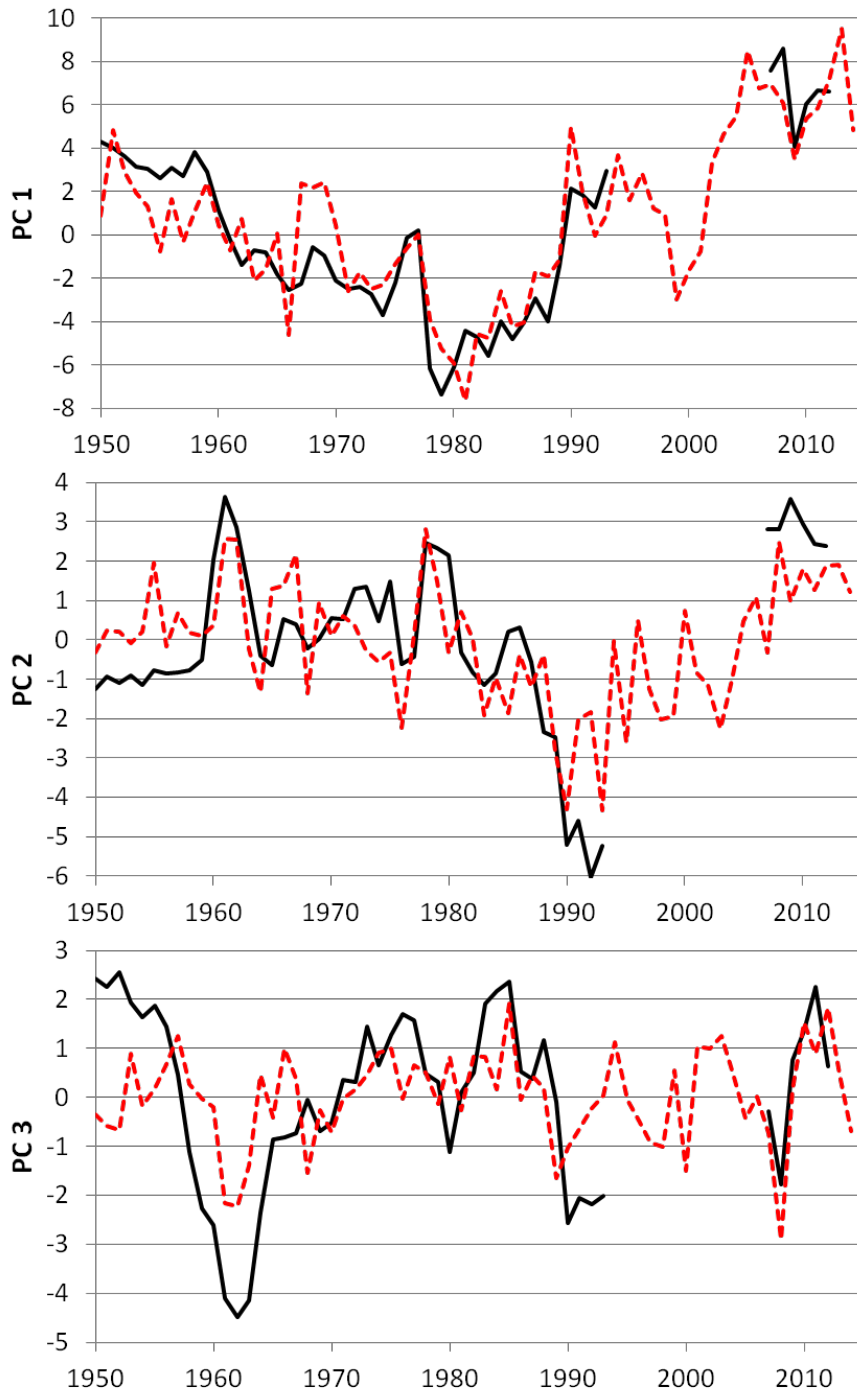


696

697 Figure 2. The average salinity field (a) and first three modes of the average salinity field

698 decomposition for the layer 5-50 m: (b), (c), (d) - 1st, 2nd and 3rd modes, respectively, for the

699 period 1950-1993 and 2007-2012.



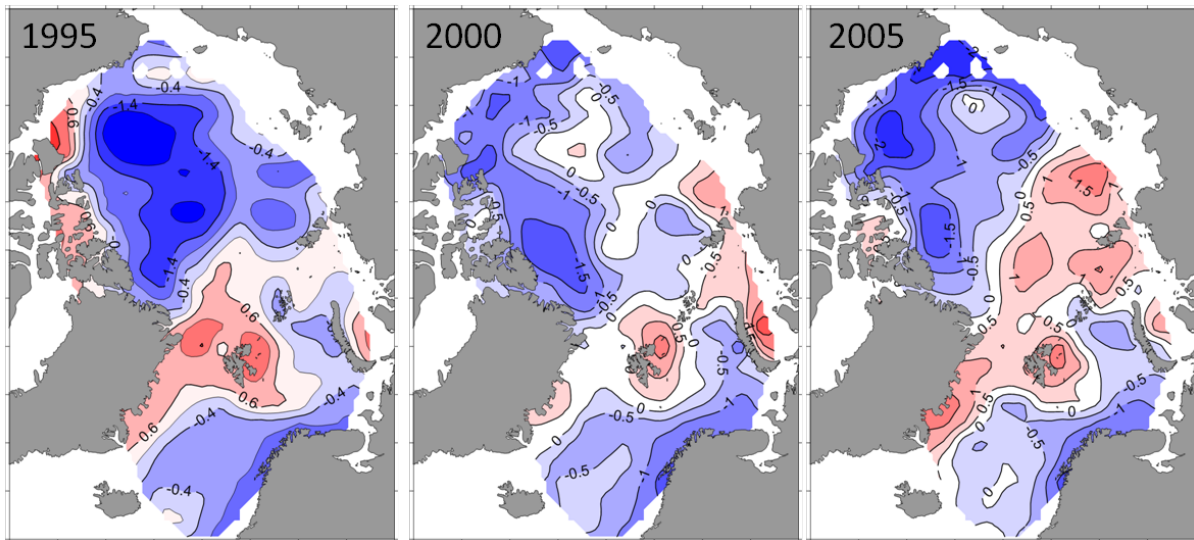
700

701 Figure 3. The actual (black line) principal components and calculated principal components

702 (red dashed line) with the help of the equations of linear regression. Correlation coefficients

703 between the calculated time series of PCs and actual PCs are: $r(PC_1)=0.88$; $r(PC_2)=0.73$;704 $r(PC_3)=0.55$.

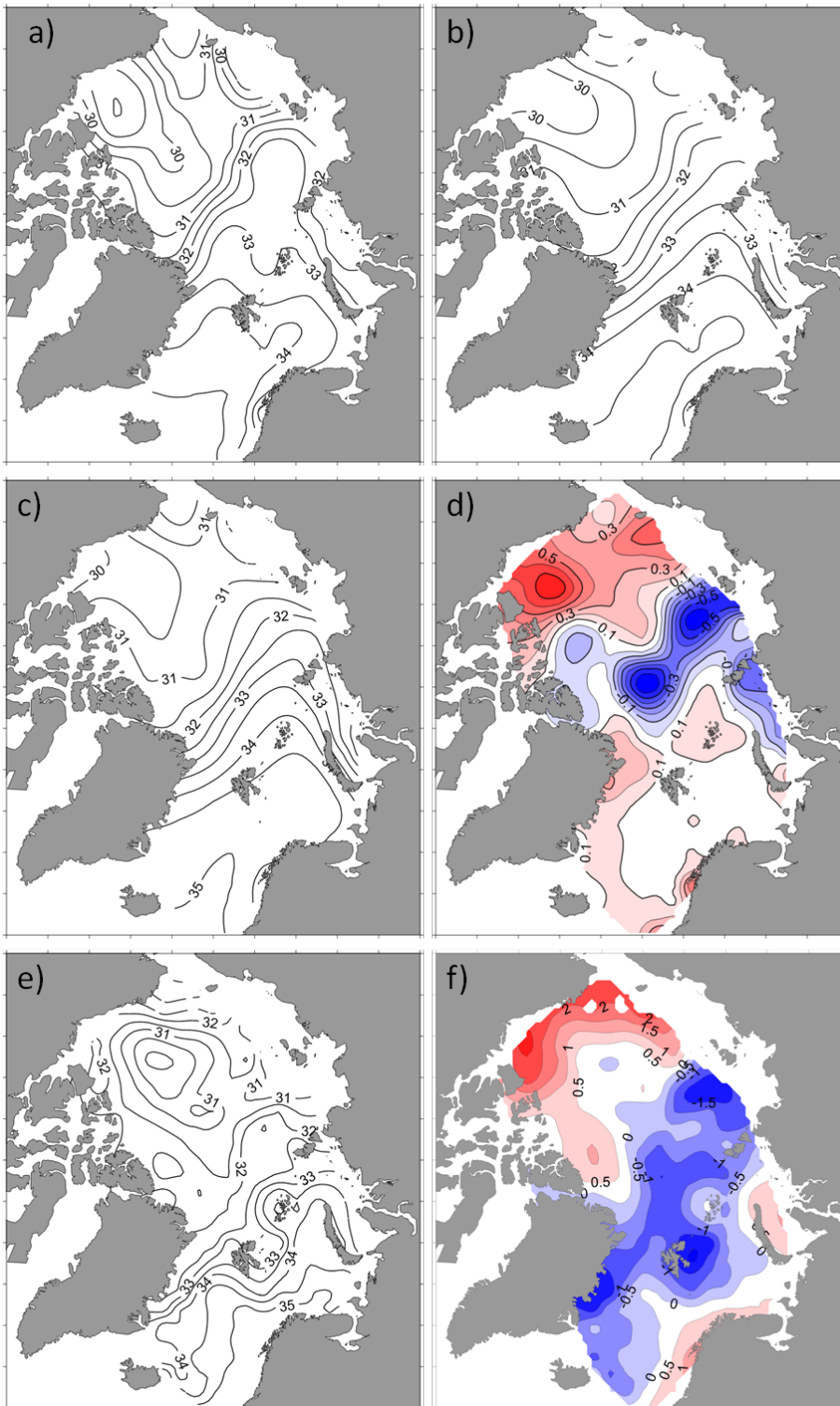
705



706

707 Figure 4. Maps of differences of salinity fields reconstructed with the statistical model and

708 those from PIOMAS data.



709

710 Figure 5. Reconstructed salinity fields for the layer 5-50 m in 2013 (a) and 2014 (b); actual
 711 salinity field for the layer 5-50 m in 2013 (c) (from AARI data), difference between actual
 712 salinity field and reconstructed one for 2013 (d); PIOMAS salinity field for 2013 (e) and
 713 difference between PIOMAS salinity field and reconstructed one for 2013(f).

714

715 **Appendix:**716 **Data and observation density**

717 Table A1. Datasets used for reconstruction and gridding of surface layer salinity fields.

718 Conventional names of regions and water areas in column 2: ArB - Arctic Basin, BaS - Barents

719 Sea, BeS - Bering Sea, BfS - Beaufort Sea, ChS - Chukchi Sea, EsS - East Siberian Sea, GrS -

720 Greenland Sea, HtR - Khatanga river mouth zone JpS - Japan Sea, KrS - Kara Sea, LpS - Laptev

721 Sea, NoS – Norwegian Sea, NrS – Nares Strait, ObR - Ob estuary zone, WhS - White Sea.

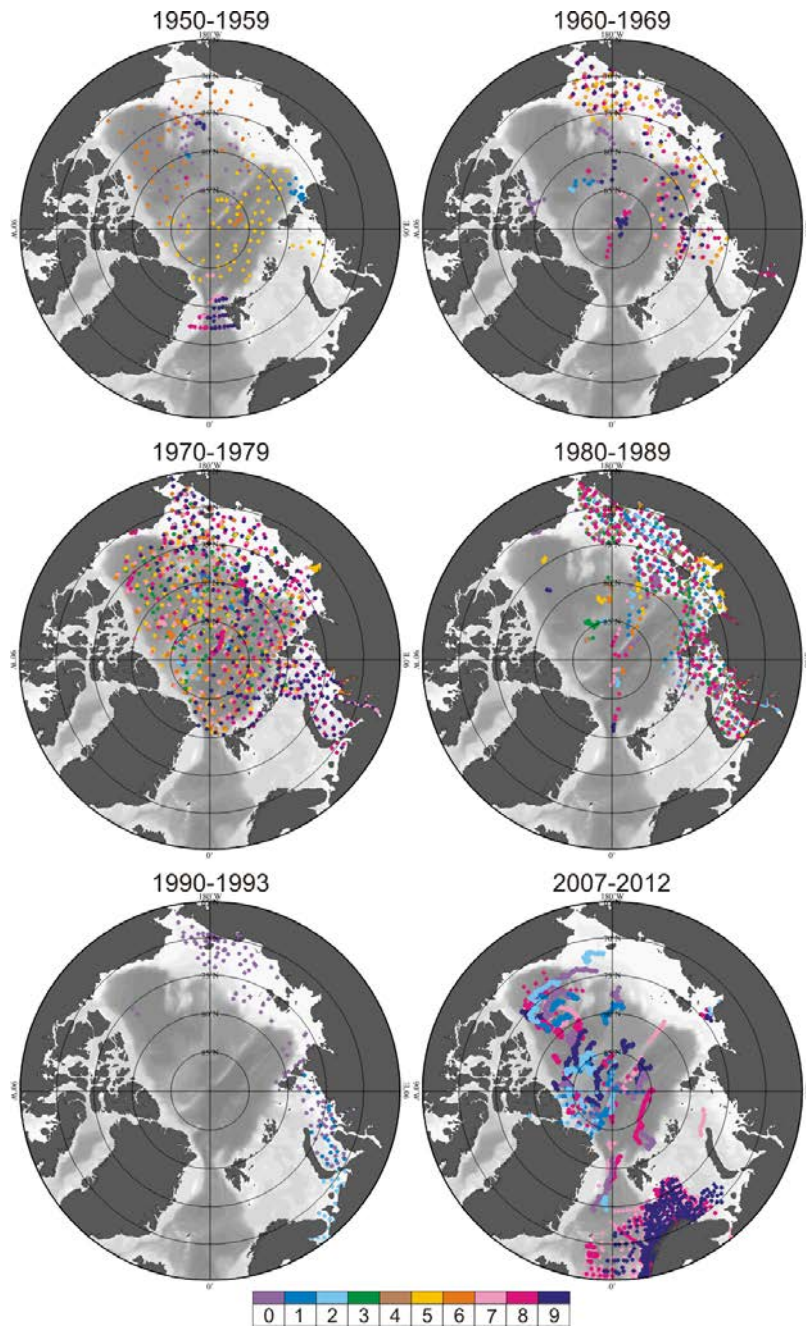
Expedition (cruise) or code of expedition	Regions, water areas	Date of station performance		Number of stations
		first	last	
SEVER05	ArB,ChS,EsS	03/31/1950	04/02/1951	51
Toros1951	KrS,LpS	04/08/1951	04/24/1951	9
SEVER07	ArB, KrS,LpS	04/16/1955	05/15/1955	105
NP05	ArB	05/20/1955	03/20/1956	14
SEVER08	ArB, ChS,EsS	04/04/1956	05/16/1956	48
SEVER09	ArB	03/1957	05/1957	11
Lena1958	GrS	03/11/1958	03/25/1958	28
SEVER10	ArB	03/1958	06/1958	18
WOD98_31_3272	ArB	03/29/1958	04/14/1958	3
SEVER11	ArB	03/1959	05/1959	30
Storm1959	GrS	04/26/1959	06/12/1959	59
NP08	ArB	06/30/1959	02/15/1962	52
SEVER12	ArB	03/1960	05/1960	27
WOD98_18_11445	ArB	04/18/1960	05/30/1960	6
WOD98_31_672	ArB	12/29/1960	12/29/1960	1
SEVER13	ArB	03/1961	05/1961	27
SEVER14	ArB	03/1962	05/1962	29
SEVER15	ArB	02/1963	05/1963	58
SEVER16	ArB,ChS,EsS,KrS,LpS	03/23/1964	05/13/1964	43
SEVER17	ArB,ChS,EsS,KrS,LpS	03/17/1965	05/11/1965	44
NP14	ChS,EsS	05/30/1965	01/24/1966	16
SEVER18	ArB,ChS,EsS,KrS,LpS	03/12/1966	05/07/1966	42
SEVER19	ArB,ChS,EsS,KrS,LpS	03/19/1967	04/26/1967	32
OBTAZ1967	KrS	04/06/1967	08/21/1967	26

NP15	ArB	04/30/1967	03/14/1968	18
SEVER20	ArB,ChS,EsS,KrS,LpS	03/19/1968	05/03/1968	60
WOD98_31_2170	ArB	03/29/1968	04/06/1968	3
AUGMS1968	KrS	04/09/1968	05/03/1968	45
NP17	ArB	06/25/1968	09/26/1969	45
SEVER21	ArB,ChS,EsS,KrS,LpS	03/18/1969	05/14/1969	95
NP16	ArB	04/22/1969	03/15/1972	83
Tiksi1969	LpS	04/25/1969	12/08/1969	51
DUGMS1970	KrS	01/06/1970	12/18/1970	73
SEVER22	ArB,ChS,EsS,KrS,LpS	03/30/1970	05/11/1970	90
AUGMS1970	KrS	04/12/1970	05/01/1970	70
NP18	ArB	05/19/1970	03/15/1971	20
NP20	ArB,EsS	05/20/1970	04/15/1972	49
NP19	ArB,EsS	11/14/1970	03/26/1973	43
DUGMS1971	KrS	01/07/1971	12/23/1971	73
Tiksi1971	LpS	01/10/1971	11/30/1971	106
SEVER23	ArB,ChS,EsS,KrS,LpS	02/28/1971	05/10/1971	81
AUGMS1971	KrS	04/19/1971	08/07/1971	112
DUGMS1972	KrS	01/06/1972	12/27/1972	95
Tiksi1972	LpS	01/10/1972	06/20/1972	54
SEVER24	ArB,ChS,EsS,KrS,LpS	02/29/1972	05/07/1972	51
AUGMS1972	KrS	04/20/1972	05/30/1972	80
NP21	ArB,EsS	05/30/1972	03/21/1974	30
SEVER25	ArB,BfS,ChS,EsS,KrS,LpS	03/19/1973	05/10/1973	178
Liman1973	KrS,ObR	03/20/1973	09/23/1973	18
Tiksi1973	LpS	05/04/1973	11/16/1973	109
Tiksi1974	LpS	12/14/1973	12/15/1974	119
DUGMS1974	KrS	01/08/1974	12/27/1974	62
SEVER26	ArB,BfS,ChS,EsS,KrS,LpS	03/11/1974	05/10/1974	166
NP22	ArB,BfS,ChS,EsS	03/23/1974	03/03/1982	117
DUGMS1975	KrS	01/04/1975	09/23/1975	145
Tiksi1975	LpS	01/15/1975	12/15/1975	55
SEVER27	ArB,BfS,ChS,EsS,GrS,KrS,LpS	03/13/1975	04/30/1975	188
DUGMS1976	KrS	01/07/1976	12/16/1977	312
AUGMS1976	KrS,ObR	02/24/1976	09/24/1976	249
SEVER28	ArB,BfS,ChS,EsS,GrS,KrS,LpS	03/11/1976	05/09/1976	155
NP23	ArB,EsS	05/30/1976	10/17/1978	83
SEVER29	ArB,BfS,ChS,EsS,KrS,LpS	03/01/1977	04/29/1977	150
AUGMS1977	KrS,ObR	03/03/1977	05/27/1977	101
WOD98_31_10614	BeS	03/31/1977	04/03/1977	16
VegaDUGMS1978	KrS	01/19/1978	12/22/1978	10
SEVER30	ArB,BaS,ChS,EsS,KrS,LpS	03/08/1978	05/10/1978	185
WOD98_31_13021	BfS	04/04/1978	07/29/1978	46

NP24	ArB	12/19/1978	09/30/1980	31
VegaDUGMS1979	KrS	01/09/1979	11/21/1979	22
SEVER31	ArB,BaS,BfS,ChS,EsS,GrS,KrS,LpS	03/02/1979	05/19/1979	205
WOD98_18_8924	BeS,ChS	04/19/1979	04/28/1979	8
VegaDUGMS1980	KrS	01/17/1980	09/26/1980	17
SEVER32	ArB,BaS,ChS,EsS,KrS,LpS	02/15/1980	05/15/1980	138
WOD98_31_10726	BfS	03/05/1980	07/02/1980	62
VegaDUGMS1981	KrS	01/06/1981	12/23/1981	32
DUGMS1981	KrS	03/17/1981	10/01/1981	344
SEVER33	ArB,ChS,EsS,KrS,LpS	03/18/1981	05/18/1981	112
VegaDUGMS1982	KrS	01/06/1982	12/29/1982	14
SEVER34	ArB,ChS,EsS,KrS,LpS	02/17/1982	05/19/1982	117
DUGMS1982	KrS	03/20/1982	05/07/1982	155
AUGMS1982	KrS	03/27/1982	06/07/1982	190
NP25	ArB	05/27/1982	03/11/1984	25
VegaDUGMS1983	KrS	01/05/1983	12/06/1983	20
SEVER35	ArB,ChS,EsS,KrS,LpS	02/25/1983	05/14/1983	235
DUGMS1983	KrS	03/22/1983	05/02/1983	67
NP26	ArB	07/01/1983	02/21/1986	35
VegaDUGMS1984	KrS	01/05/1984	11/26/1984	24
AUGMS1984	KrS	01/06/1984	12/24/1984	175
TUGKS1984	LpS	01/15/1984	12/27/1984	112
SEVER36	ArB,ChS,EsS,KrS,LpS	02/27/1984	05/13/1984	247
TUGMS1984	EsS,LpS	03/23/1984	05/22/1984	20
DUGMS1984	KrS	04/01/1984	05/18/1984	36
Pevek1984	EsS	04/10/1984	12/29/1984	37
NP27	ArB,EsS	06/26/1984	03/10/1987	35
TUGKS1985	EsS,LpS	01/03/1985	09/24/1985	213
VegaDUGMS1985	KrS	01/03/1985	12/24/1985	20
Pevek1985	EsS	01/10/1985	03/29/1985	17
SEVER37	ArB,ChS,EsS,KrS,LpS	02/25/1985	05/10/1985	296
TUGMS1985	EsS,LpS	03/21/1985	05/04/1985	39
WOD98_31_12556	BfS	04/01/1985	04/18/1985	7
DUGMS1985	KrS	04/02/1985	09/20/1985	209
AUGMS1985	KrS	04/05/1985	07/01/1985	38
VegaDUGMS1986	KrS	01/06/1986	12/26/1986	22
SEVER38	ArB,ChS,EsS,KrS,LpS	02/26/1986	06/06/1986	196
DUGMS1986	KrS	04/03/1986	08/24/1986	96
SEVER39	ArB,ChS,EsS,KrS,LpS	02/25/1987	06/08/1987	284
NP28	ArB,GrS	05/07/1987	01/17/1989	34
SEVER40	ArB,BeS,ChS,EsS,LpS	03/09/1988	05/19/1988	282
AUGE1988	HtR,LpS	05/06/1988	09/19/1988	100
SEVER41	ArB,BeS,ChS,EsS,LpS	02/27/1989	06/02/1989	262

NP31	ArB,BfS	06/29/1989	03/26/1990	10
SEVER42	BeS,ChS,EsS	01/19/1990	08/11/1990	150
SEVER43	KrS	04/25/1991	05/24/1991	20
SEVER44	ArB,BeS,ChS,EsS,LpS	02/27/1992	06/02/1992	206
SEVER45	BaS,KrS,WhS	04/08/1993	06/14/1993	180
CELTIC VOYAGER	NoS	04/07/2007	04/07/2007	1
CLUPEA	NoS	05/10/2007	05/12/2007	57
LLZG (G.O. SARS)	NoS, BaS	02/07/2007	11/26/2009	350
HAKON MOSBY	NoS, GrS	01/10/2007	12/05/2009	989
HERWIG, W.	NoS	02/07/2007	01/10/2007	14
ITP01	Bfs	01/01/2007	01/08/2007	32
ITP04	ArB	01/01/2007	05/31/2007	302
ITP05	ArB	01/01/2007	05/31/2007	453
ITP06	ArB	01/01/2007	05/31/2008	580
ITP07	ArB	04/28/2007	11/01/2007	134
LDGJ (JOHAN	BaS, GrS, NoS	01/15/2007	12/04/2009	1178
MAGNUS	NoS	02/15/2007	11/10/2008	364
Transarctica_2007	ArB, LpS, KrS	05/15/2007	05/31/2007	49
SCOTIA	NoS	01/29/2007	02/14/2010	288
Tara	ArB	01/13/2007	12/10/2007	35
Twin Otter	ArB	04/21/2007	05/07/2007	10
CELTIC	NoS	05/21/2008	05/21/2008	3
TRANSDRIFT XIII	LpS	04/10/2008	05/05/2008	17
ITP08	ArB	01/01/2008	05/31/2008	303
ITP09	ArB	01/01/2008	02/27/2009	408
ITP10	ArB	01/01/2008	05/25/2008	293
ITP11	ArB	01/01/2008	05/31/2009	630
ITP13	ArB	01/01/2008	05/31/2008	317
ITP16	ArB	01/01/2008	04/03/2008	140
ITP18	BrS	01/01/2008	05/31/2008	317
ITP19	ArB, GrS	04/08/2008	11/21/2008	216
LAHV (JAN	BaS	02/07/2008	03/06/2009	304
NP35	ArB	01/01/2008	12/31/2008	152
NPEO_2008 (Twin	ArB, BfS	03/21/2008	04/20/2008	43
TRANSDRIFT XV	LpS	03/24/2009	04/23/2009	15
HERWIG, W.	NoS	02/10/2009	02/15/2009	16
NP36	ArB	01/01/2009	12/31/2009	151
ITP21	ArB	01/01/2009	05/31/2009	288
ITP23	ArB	01/01/2009	05/31/2010	599
ITP24	ArB	01/01/2009	05/31/2009	299
ITP25	ArB	01/01/2009	05/31/2009	298
ITP26	ArB	01/01/2009	02/26/2009	114
ITP27	ArB	01/01/2009	01/20/2009	40

ITP29	ArB	01/01/2009	05/31/2010	589
ITP33	BfS, ArB	01/01/2010	01/25/2011	351
ITP34	BfS, ArB	01/01/2010	05/31/2010	298
ITP37	ArB	01/01/2010	12/24/2010	301
ITP38	ArB, GrS	04/19/2010	12/28/2010	170
NP37	ArB	01/01/2010	12/30/2010	112
NPEO_2010	BfS	05/25/2010	05/26/2010	4
NPEO_2011(Twin	ArB	04/28/2011	05/08/2011	25
ITP41	ArB	01/01/2011	05/31/2012	607
ITP42	BfS, ArB	01/01/2011	04/15/2011	201
ITP43	BfS	01/01/2011	02/11/2011	83
ITP47	ArB	04/11/2011	02/28/2012	434
PALEX 2011	ArB	04/10/2011	04/20/2011	20
NP38	ArB	01/01/2011	11/01/2011	147
BARNEO2012	ArB	04/06/2012	04/17/2012	24
ITP48	ArB	01/01/2012	11/16/2012	446
ITP53	BfS	01/01/2012	05/31/2012	304
ITP55	ChS	01/01/2012	05/08/2012	257
ITP56	ArB, GrS	04/15/2012	12/31/2012	185
ITP63	ArB	04/21/2012	12/31/2012	161
NP39	ArB	01/01/2012	12/31/2012	143
SWITCHYARD2012	ArB, NrS	05/03/2012	05/21/2012	23
TRANSDRIFT XX	LpS	03/26/2012	04/19/2012	7
All expeditions	All regions	03/31/1950	12/31/2012	24557



722

723 Figure A1. Observation density. Color bar indicates the last number of the year in each decade.

724 The total number of observations in the 1950s – 428, 1960s – 751, 1970s – 3837, 1980s – 4374,

725 1990s – 556, 2000s – 14691.

726

727

728

729 **The empirical equations for the first three principal components**

730 The equations are derived from the formula for multiple linear regression

731
$$y_i = \sum a_{ij} x_{ij} + b_i \quad (A1)$$

732 where the y_i are the principal components PC_i ; the x_{ij} are variables independent of the y_i (the733 different environmental factors), the a_{ij} are regression coefficients, and the b_i are the

734 intercepts. To determine which predictors to include in each regression model, we used the

735 “forward stepwise” method. Each predictor leads the salinity EOF by some number of years,

736 and these temporal lags were determined to maximize the variance accounted for by each

737 predictor.

738 The values of the correlation coefficients (R), coefficients of determination (R^2) and F-

739 criteria (Hill and Lewicki, 2007) are presented in Table A2. The values of all F-criteria exceed

740 the threshold indicating that the models are statistically significant. The correlation coefficients

741 for all PCs were statistically significant and varied from 0.55 (R_3) to 0.88 (R_1).

742

743

744

745

746

747

748

749

750

751

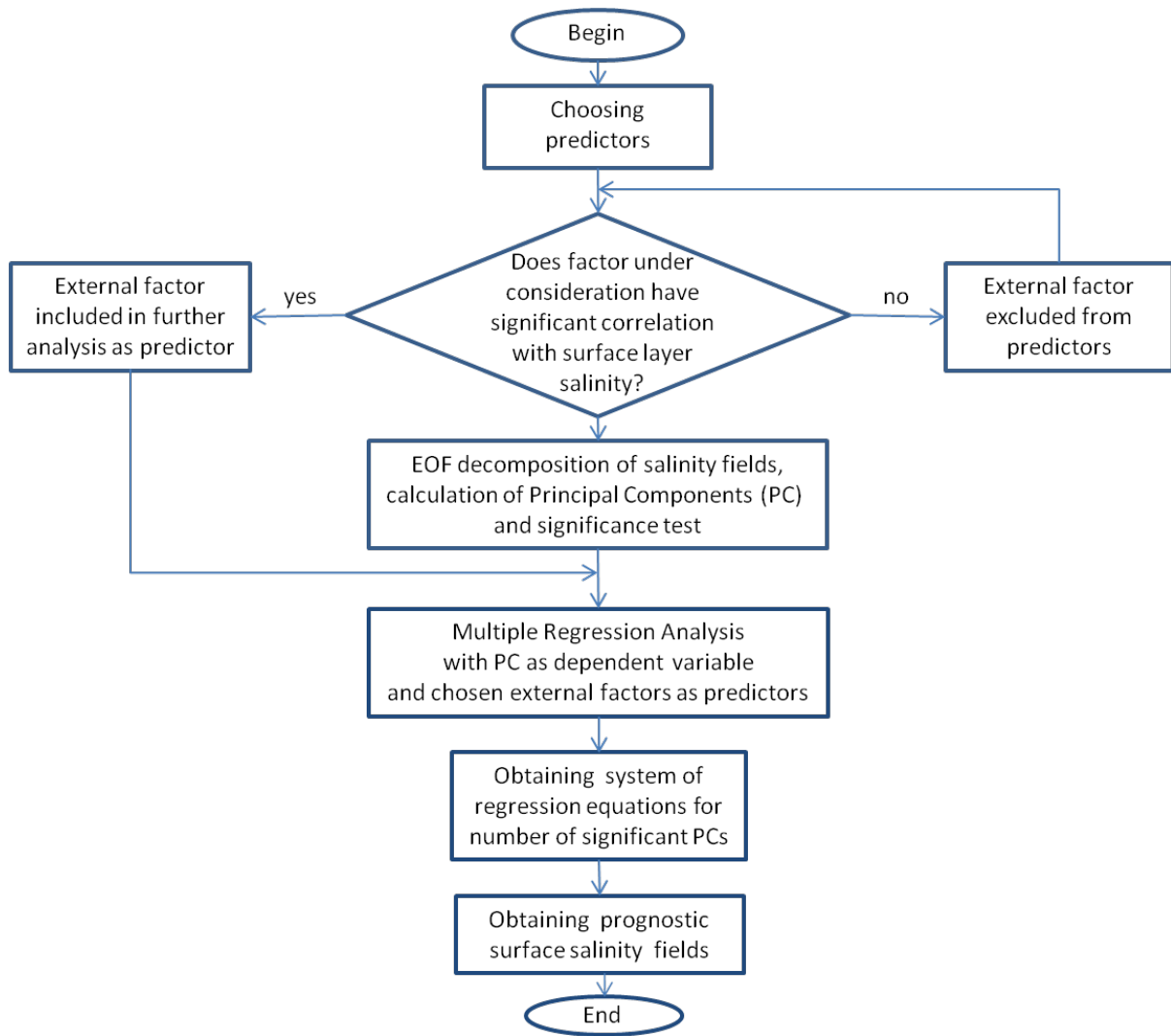
752

753 Table A2. The empirical statistical model developed for each of the first three PCs. The lower case indicates the months of an averaging period or
754 the first letters of the sea name (see Table 1).

PC_i	Statistical Equations	Multiple R	Multiple R^2	Adjusted R^2	F- criteria
PC ₁	$PC_1 = 11.60 \times AMO(-7)^* + 0.008 \times OW_{EC}(-1) + 1.28 \times PDO(-10) + 1.86 \times AO_{VII-IX}(-1) - 7.87$	0.88	0.78	0.76	40.07 (4;45)**
PC ₂	$PC_2 = -1.28 \times AO_{VII-IX}(-1) + 1.22 \times AD_{VII-IX}(-1) - 1.18 \times PDO(-6) + 0.008 \times RIV_{LEC}(-4) - 8.07$	0.73	0.53	0.49	12.81 (4;45)
PC ₃	$PC_3 = -0.97 \times AD_{X-III}(-1) - 4.00 \times AMO(-10) - 0.68 \times PDO(-3) + 0.004 \times RIV_{LEC}(-5) - 4.82$	0.55	0.30	0.23	4.76 (4;45)

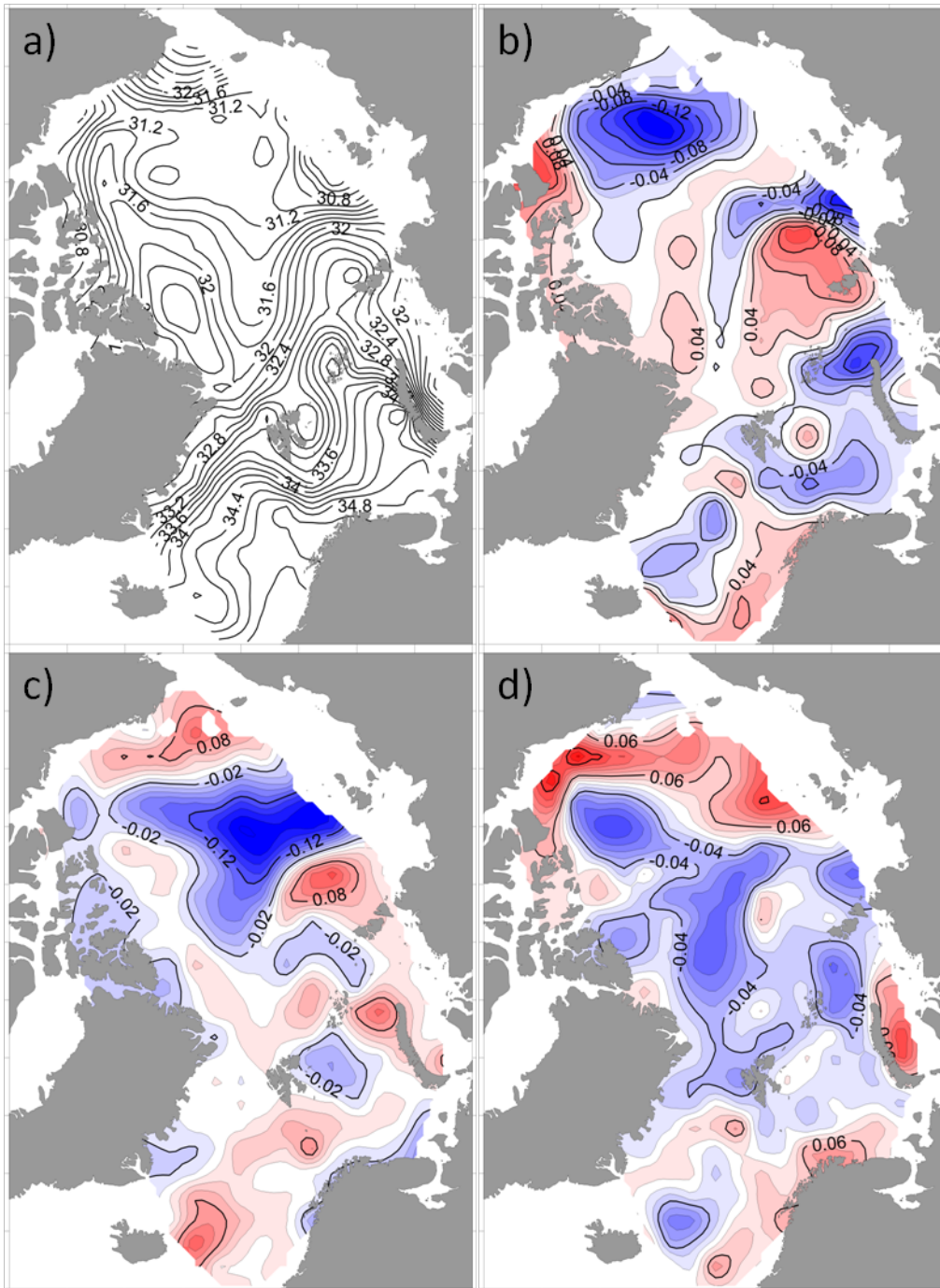
755 * – time shift for every predictor is indicated in parentheses (minus means that predictor leads the dependent variable).

756 ** – numbers of degrees of freedom are indicated in parentheses.



757

758 Figure A2. Schematic diagram of the conceptual statistical model.

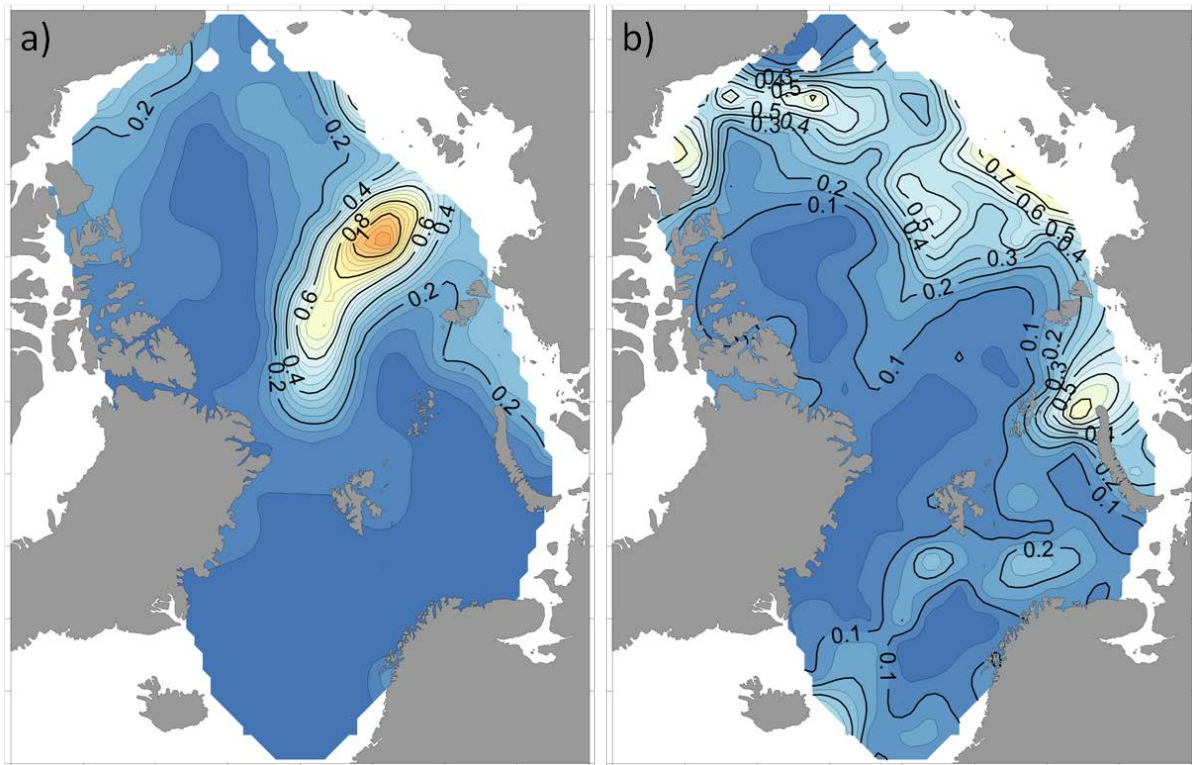


759

760 Figure A3. Same as Figure 2, but for salinity averaged annually over the upper 50 m of

761 PIOMAS data for 1978-2012.

762



763

764 Figure A4. Variance maps of surface layer salinity for the 1978-2012 period: a) – AARI data

765 base, b) – PIOMAS data.

766